University of Stavanger

SANDER HARBO
SUPERVISOR: FREDRIK BJØRHEIM

Assessment of Mechanical Properties of 17-4 PH Stainless Steel Printed By Bound Metal Deposition (BMD)

Bachelor thesis, 2024

Structural engineer

Faculty of Science and Technology

Department of Mechanical and Structural Engineering and Materials Science

Abstract

Additive manufacturing (AM) is a modern technology that can produce parts from a 3D model by iteratively building the part layer by layer. Some of the benefits of using AM are reduced delivery times, storage needs, and design freedom due to AM being able to produce parts not possible using conventional methods. On the other hand, many well-known defects and residual stress are found in most AM methods. A newer AM process called Bound Metal Deposition (BMD) utilizes a different printing process that is significantly cheaper, easier to operate, and is expected to have almost no residual stress. However, significant defects running parallel to the printing lines have been identified in BMD. This thesis aims to investigate how these defects influence mechanical properties and fatigue capacity, with particular emphasis on variations across different printing orientations. The literature review showed that the mechanical properties of BMD, as well as those of powder bed fusion and direct energy deposition, depended on the direction of the defect relative to the applied force. Specimens, where the defects were parallel with the applied force, had the best mechanical properties, and specimens, where they were perpendicular, had the worst. Additionally, testing performed for this thesis found that specimens whose defects were at a 45-degree angle to the applied force were stronger than those with defects parallel to the printing direction, perhaps due to the mesh created by the lines changing direction iteratively layer by layer. Furthermore, a thorough interpretation of the effect of the defects on fatigue capacity found that the defects are prone to crack initiation and that vertically printed specimens are likely to have the worst fatigue capacity.

Acknowledgment

I wish to express my profound gratitude to Fredrik Bjørheim, my thesis supervisor, for his invaluable guidance and support. I also want to give my sincere thanks to Jan-Tore Jakobsen for his help with manufacturing the testing components, and for his steadfast support during unforeseen challenges. Finally, I take this opportunity to thank Joar Haaland for generously providing office space at Subsea 7 which enhanced my productivity throughout the writing process.

Table of contents

1. Introduction

Additive manufacturing (AM), also known as 3D printing is a technology in which a part is iteratively built layer by layer following a digital computer-aided design (CAD) model. This makes it possible to produce complex, and completely customized parts directly from the design without the use of expensive tooling, and the limitations of conventional processing steps[1]. AM can even produce parts that are impossible to produce with the use of more traditional means such as casting and subtractive manufacturing. With the use of AM, economy of scale does not apply, making it exceptional at producing individual products and short production series, as the setup cost for a new part is relatively low [2]. There are several methods of AM, with some of the most commonly used being powder bed fusion (PBF), and direct energy deposition (DED) [3]. With the different methods, there are different printing parameters, and the choice of printing method, and printing parameters will highly affect the resulting product [1].

AM can lead to more sustainable and cost-effective production by moving it to where the product is needed, which reduces transportation time, emissions, and the need for warehouses [2]. Today it is common for companies to order and store parts from countries far away, creating emissions from long transport routes and the need for warehouses as they order a quantity of parts each time. Companies such as Equinor have already implemented a digital inventory together with their on-site AM facility to reduce warehousing, transportation time, and emissions. Furthermore, a digital inventory makes it possible to print the part locally when it is needed instead of storing many excess parts. Additionally, this way they can purchase a design from anywhere in the world and print it on-site. Equinor's plan for the next three to five years is to reduce physical warehousing by 25% and in ten years by 50%. Furthermore, Equinor managed to produce parts that would normally take up to 40 weeks due to long delivery times, in just 10 weeks using their own AM facilities [4]

Another thing making AM a more sustainable option is the expanded possibilities for repair. With technology to scan broken parts, it is possible to scan, redesign, and 3D print any part that is broken or missing. In fact, Siemens claims that using AM reduced repair time for certain burner tip models by around 90% by printing the replacement part directly onto the body of the burner [5].

Although there are many benefits and possibilities for AM, there are several improvements to be made both for the mechanical properties and economic perspective. Known defects are loss of alloying elements, lack of fusion, surface roughness, cracking, delamination, and residual stresses [1]. Many of these defects lead to reduced or changed mechanical properties, including deterioration of the fatigue performance, as opposed to wrought counterparts [1]. It is highly relevant to find methods that show better qualities in these areas. In addition, the cost of setting up and running AM production is high and requires specific safety equipment [6]. The industry may respond well to a cheaper and more user-friendly system.

Bound Metal Deposition (BMD) is a newer method that shows improvements in several of the challenges with AM including a possible reduction in residual stress, lower cost, and a system that is simpler to use. Research on BMD is limited, and this thesis aims to find the effect defects found in BMD have on the mechanical properties and fatigue capacity. Special attention has been given to finding the effect of defects for different printing orientations. Findings will be compared to conventionally manufactured (CM), PBF, and DED specimens. To provide a basic understanding of AM and necessary theory, this paper includes a literature review of the most common AM processes and the effect of defects found in these AM processes. Furthermore, the theory of Fatigue capacity and the theory of tensile- and fatigue testing are included. In addition, tensile testing was conducted on BMD specimens, and results were presented and discussed. The effect of defects on fatigue capacity will be addressed, and an optical light microscope picture will be used to present and interpret the defects.

2. Literature Review

2.1. Defects and Residual Stress in AM

The printing processes in AM lead to several defects. One of them is the loss of alloying elements from vaporization due to hot temperatures, leading to notable changes in the final alloy composition. Other problems are the lack of fusion in the shape of coin-like voids with sharp edges and delamination between layers, which both can experience stress concentration if force is applied perpendicular to the defect. Consequently, the edge of the void can experience stress two or three times more than other parts of the material. Moreover, there are pores, surface roughness, and cracking, which are also prone to stress concentrations. Overall, many defects in AM need to be considered when designing parts as they can greatly influence mechanical properties such as tensile strength and fatigue capacity [1].

Fatigue is the cyclic loading of a material, a type of loading that will be further explained in Chapter 3.1. The first stage of fatigue failure is crack initiation, which typically occurs where there are stress concentrations. The rough surface of AM is frequently recognized as a common site for crack initiation, along with lack of fusion areas and pores [7]. In addition to these defects, residual stress affects fatigue capacity, tensile capacity, and other mechanical properties. Several factors, such as high thermal gradients, high energy density, and most importantly, fast solidification during AM processes, can cause residual stresses in AM parts. When new layers are deposited, stress gradients can occur because of rapid heat transfer induced by the heat source leading to thermal expansion and contraction of material [8]. As a result, the material is exposed to stress before being affected by an external force, meaning that once force is applied to the material the residual stress will add to the total stress experienced by the material [9]. Residual stress can often be found near the surface, which is detrimental when combined with the stress concentrations occurring due to a rough surface. Furthermore, delamination between layers is frequently created by residual stress exceeding the yield strength of the material [1].

2.2. Post Processing

Different thermal post-processing treatments have been proven to positively affect AM's mechanical properties. Hot isostatic pressing (HIP) is a frequently used thermomechanical method where specimens are heated up to temperatures between 1000-2000 °C while, at the

same time, pressure is applied uniformly. This method can have a profound effect on the mechanical properties as it homogenizes the microstructure, alleviates residual stress, and closes pores as well as the more minor lack of fusion defects. A combination of a more homogeneous microstructure together with less residual stress leads to better fatigue capacity [10], [1].

Another effective measure towards bettering mechanical properties is to machine the rough surface. This will subsequently reduce surface roughness and minimize crack initiation sites, which will improve fatigue capacity and other mechanical properties[1], [10].

2.3. Powder Bed Fusion

There are two distinct methods of Powder Bed Fusion (PBF), and the distinction is made in what heat source is used in the printing process. Selective Laser Melting (SLM) and Selective laser sintering (SLS) uses a laser as the heat source, while Electron Beam Melting (EBM) uses an electronic beam [1],[11].

The powder bed fusion methods SLM and SLS involve evenly distributing metal powder to a powder bed by using a roller, wiper, or doctor blade. A laser will then scan the selected location and fuse the metal powder. Once one layer is fused the powder bed is lowered by the defined thickness and another layer of metal powder is distributed. The laser fuses the powder iteratively, layer by layer until the part is finished [11].

Electron Beam Melting works much in the same way, but it utilizes an electron beam instead of a laser. The beam will first slightly sinter the powder bed, before sintering the given part volume. This is to prevent electro-static charging and repulsion of the powder particles, but it also allows for a faster scanning speed as the metal powder is already slightly sintered [1].

A general figure of the PBF method can be seen in Fig 1.

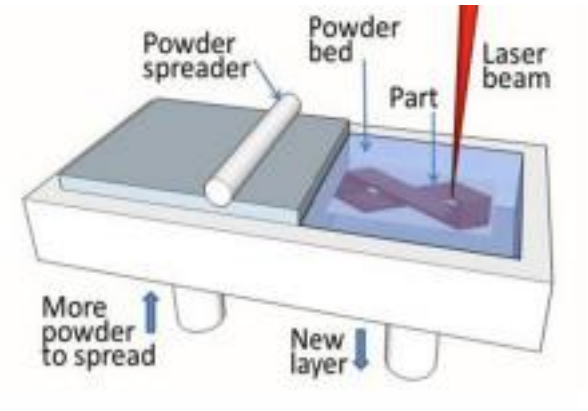

Fig 1 Powder Bed Fusion [1]

With PBF there are many opportunities. PBF allows for many scanning patterns, also known as hatching, such as unidirectional, bidirectional, spiral, zigzag, and crosswise. These changes in scanning patterns can directly affect the mechanical properties of the finished part, as the microstructure of PBF parts is known to be related to the direction of printing. The printing process also makes it possible to print multiple parts in one build cycle if there is room on the powder bed, making it efficient in producing many parts. Furthermore, the parts produced from PBF show a good surface finish as well as good dimensional accuracy, which also means that the finished part requires little post-processing to achieve the desired shape and accuracy. On the other hand, the limitations of the powder feeding rate and scanning speed together with low layer thickness make the production time of PBF high, and the use of a powder bed means that much of the non-sintered metal powder is reused, which can lead to poor surface finish and higher costs due to handling of the powder [1].

Powder bed fusion is known to have directional-dependent mechanical properties. This can be explained by the melting pool that happens during printing due to extreme temperature gradients and the fast melting and solidification this creates, leading to columnar crystals forming between melting pools in the printing direction [12]. Yang [12] found that the ultimate tensile strength (UTS) and elongation of SLM printed Cu-10Sn specimen were highest when printed horizontally, lowest when printed vertically, and with various results in between for different angles. His theory was that the grain boundaries would be closer in the horizontal specimen, making it harder for dislocations to migrate, leading to less deformation and thus improving the strength. The specimens were stronger and more ductile when force was applied perpendicular to the columnar grain. In addition, Yadollahi [13] found that

printing direction played a significant role in fatigue capacity, with nonmelted regions due to the lack of fusion between layers being the most critical defect. The stress concentrations around the lack of fusion will be the highest when force is applied perpendicular to the defect.

Much testing has been done to compare different mechanical properties of PBF specimens to conventional manufactured (CM) specimens. Nezhadfar [14] performed tensile and fatigue testing of specimens printed using selective laser sintering (SLS) and 17-4 PH stainless steel as printing material and compared the results to those of CM specimens. It was found that the tensile capacity was comparable to its wrought counterparts, as reported in the ASTM A693 standard [15]. The as-sintered specimens had a lower UTS and yield strength, but the CA-H900 heat-treated specimens achieved higher UTS and yield strength than their wrought counterpart. Fatigue testing showed that wrought specimens had better fatigue performance than the as-built AM specimens. Still, the fatigue life of SLS specimens improved significantly when the rough surface was removed with machining. Similar results were obtained by Carneiro [16] when comparing SLS parts to wrought counterparts. He reported that cracks in the SLS parts were initiated on the rough surface of the as-sintered SLS part. Furthermore, Sarkar [17] performed a Vickers hardness test and found that SLS specimens were harder than CM 15-5PH stainless steel specimens. He also found that heat treatment made both SLS and CM parts harder. This increase in hardness can be explained by the smaller grain size and the microstructure distribution obtained by heat treatment, making dislocations and plastic deformation more challenging [18]. Sanjeev [19] also found that SLS specimens were harder than CM specimens. He attributed this to the finer microstructure of SLS, which develops due to the high cooling rate in the printing process. On the contrary, Eisazadeh [17] conducted Vickers hardness tests for 17-4PH stainless steel where CM specimens were harder than SLS-produced specimens, showing that SLS is not always harder. Eisazadeh also found that the hardness of SLS specimens increased the most, which can be attributed to the overall grain size reduction being larger in SLS specimens than in CM.

2.4. Direct Energy Deposition (DED)

Direct energy deposition (DED) utilizes different power sources such as laser, electron beam, and plasma arc, which melt material deposited by feeding commercial filler or by precisely blowing metal powder through the power source. This metal is ejected through a nozzle and onto the part layer by layer, following geometry from a computer-aided design (CAD) file. It

is possible to control the power source's energy density and the powder deposition density [1]. An illustration of the process can be seen in Fig 2**.**

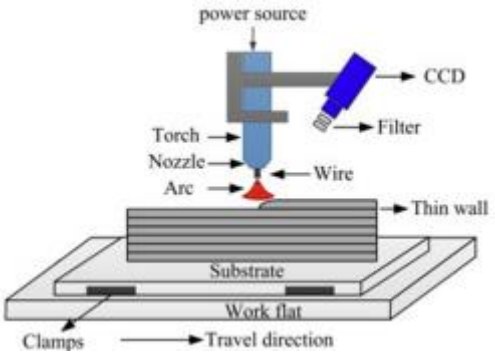

Fig 2 DED Printing process [1]

The DED method, which utilizes a laser beam as the power source, is called direct material deposition (DMD) or laser-engineered net shape (LENS). An illustration of this method can be seen in Fig 3**.** Yet another DED method that utilizes an electronic beam as the power source is commonly referred to as electron beam freedom fabrication (EBF3) or electron beam additive manufacturing (EBAM), which is illustrated in Fig 4**.** The last DED method utilizes an electric arc as the power source and is most referred to as (PA-DED) [1], [20], [21].

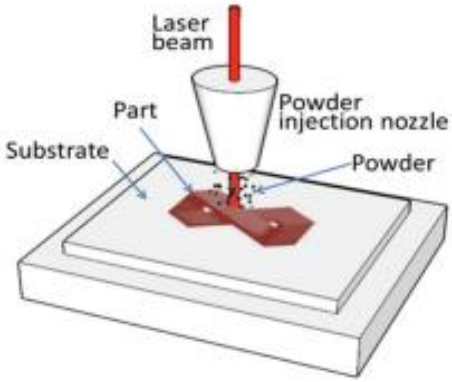

Fig 3 DED – Laser [1]

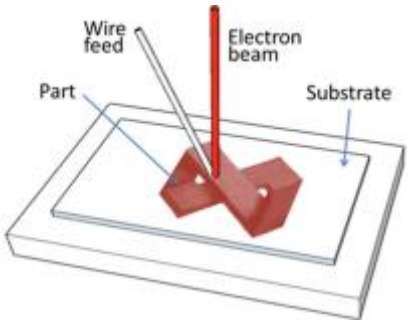

Fig 4 DED Electron Beam [1]

Direct energy deposition offers several advantages, such as fast deposition, meaning that a part can be made quicker than in PBF, which leads to DED being suitable for printing larger parts. DED also provides the opportunity to print onto existing parts and print multiple materials during the building process, making it great for repair. Furthermore, the use of wire metal as opposed to powder makes for easier storage and fewer safety hazards. However, large weld beads are required to print fast, resulting in a rougher surface that requires more post-processing to achieve the desired shape. In addition, the parts cannot be as complex and cannot have large overhangs. Residual stress is also highly present in DED, which can lead to distortion as well as reduce mechanical properties [1], [20].

As for PBF, the mechanical properties of DED are also dependent on the printing direction due to columnar grains occurring parallel to the printing direction [22]. Lu [22] found that specimens tested with the columnar grain perpendicular to the applied tensile force showed high strength and low elongation, whilst specimens where the columnar grain was parallel with the applied tensile force showed low strength and high elongation. Similar results were found by [23], who reported similar UTS for horizontal and vertical specimens but a distinct difference in elongation, where specimens with the columnar grain parallel to the applied tensile force experienced more elongation.

Johnson [24] tested DED-printed specimens using Inconel 718 as material. He found that the fatigue life was shorter than that of its wrought counterparts and that the major cause for the shorter fatigue life is most likely the pores/particles that occur in the printing process. Tang [25] also found a clear correlation between fatigue life and pores. He found that when plotting the effective size of the pore, distance from pore to surface, and the fatigue life, there was a clear trend for fatigue life to be short where the pores were big and distance to surface short,

but longer when the pores were small, and the distance to surface was long. Furthermore, Tang [25] also found a correlation between printing orientation and fatigue life, with horizontally printed specimens having, on average, twice the fatigue life of vertical specimens. One key factor presented as the reason for this was the difference in columnar grain orientation.

Muslim [26] found that for 17-4PH stainless steel, the hardness was well within the expected limits and even above the numbers given in AMS2759 for hardness after different heat treatments. Furthermore, he found that energy density in the printing process also played a crucial role in the hardness of the finished part. Higher energy density resulted in a lower hardness of the finished part due to grain structure coarsening from a higher energy density.

2.5. Bound Metal Deposition (BMD)

Bound Metal deposition, also known as bound powder extrusion (BPE) or atomic diffusion additive manufacturing (ADAM), is a technology for additive manufacturing that has proven to have several advantages over other AM technologies. One of the advantages is that costs are roughly 60% less than similarly sized PBF facilities. This can be a deciding factor for many companies that are looking into using AM in their production. Furthermore, the facilities where BMD is performed do not need suction and controlled ventilation, and the workers do not need to wear specific safety equipment, as the material cannot be inhaled, and it is not dangerous to get in contact with the metal. In contrast, the metal powder used in the PBF method is characterized by a flammable and volatile behavior due to the very small size of the metal [6]. Additionally, the storage conditions of this metal powder are critical for the mechanical properties of the finished product [27]. All these challenges with the use of metal powder do not apply to BMD as the metal powder used in BMD is bound in a composition of wax and polymer binder.

Unlike in other AM technologies, the BMD process does not sinter layer by layer. Instead, the part is sintered once it is fully printed, which effectively eliminates the problems caused by fast solidification that often lead to high residual stresses within the finished product [3]. As BMD does not create a melting pool around the heat source, the microstructure is not expected to be characterized by column or cell dendrites. In fact, Todd C. Henry found that the microstructure can be compared with the microstructure that would be expected in heat-treated commercially available 17-4PH stainless steel [28]. The lack of a melting pool also indicates that alloying elements should not be lost in the printing process.

2.5.1. Printing Process BMD

The printing process of BMD can be separated into four parts. Printing, de-binding, sintering, and post-processing. First, a 3D design is made as an STL file, and using software, the user can decide various parameters, including printing direction, material, layer height, number of walls, and fill pattern. This level of control empowers the user to optimize the printing process according to their specific needs. The software will then automatically account for the shrinkage during sintering before sending the dimensions to the printer. Supports will automatically be created where necessary, and a raft can be added under the part to ensure proper shrinkage without warping during printing. [29].

The material used to print comes in the form of metal powder being held together by wax and polymer binder in a wire spool. This rod is then heated up, allowing it to be extruded through a designated nozzle that prints following the model's geometry. When printed like this, the user will not be exposed to metal powder, lasers, or beams. The printer will print walls following the geometry parameter and then print the fill-in part. It will print this way iteratively, layer by layer until the shape is completed. It is possible to choose between 2-8 layers of walls, and the infill can be solid, triangular, or gyroid. These choices may influence the weight and mechanical properties of the finished product. Once the part is printed, it is called a green part [29].

The green part is now ready for the de-binding process. In this process, the wax binder will be removed, creating an open-pore structure that leaves room for the polymer binder to escape during sintering [30], [31]. De-binding involves emerging the part in a solvent for several hours, with the time it takes depending on the thickest part of the printed specimen [30]. It is important to think of the de-binding process when designing the part, as the processing time is highly affected by the thickness of the part [32]. Once the de-binding is finished, the part is called a brown part and is ready to be sintered.

The sintering happens in a sinter where the temperature is raised to around 1300 degrees for typically between 26 and 31 hours [31]. A vacuum is then created, and the sinter is filled with an inert gas of 97.2% Argon and 2,8% Hydrogen [33]. In this process, metal particles are fused and shrink between 17% and 22%, meaning understanding and controlling the shrinkage is crucial to achieving accurate dimensions. To achieve this accuracy, dilatometry is used to tune the sintering cycle to achieve repeatable shrinkage and densification [30]. It is important to consider if the part needs additional support to prevent it from buckling, warping,

or collapsing in the sinter. This is due to the friable nature of the brown part [34]. If a cantilever section of the part is left without support, the weight of the section can be enough for it to deform as it heats up. After sintering, the part is ready to be used “as sintered” or further processed. If the edges of BMD parts are machined, it is important not to remove too much material as it risks removing the outer layer (walls) of the part [29].

2.5.2. Earlier Testing of BMD

Defects

Bjørheim and Lopez [3] found defects that are directly correlated to the printing orientation. Between each printed line, there is a parallel defect of missing material that can be explained by the nozzle's inability to print each line as a perfect square. Two lines with a non-rectangular cross-section after one another will leave room in between. When there are several such printing lines, a mesh of longitudinal defects will appear, as seen in Fig 5, which presents how the defects appear in the plane between two printing layers. The defects from the infill cannot be seen in the figure but should be similar, only at a 45-degree angle to the defects seen. The infill defects will change direction iteratively layer by layer, as illustrated for a small section using red and green lines in Fig 5. Cross-sections of the defects are seen as both square and triangular holes. The square holes are defects in the wall section of the print, as seen in Fig 6, and the triangle holes are defects from the solid fill-in, as seen in Fig 7**.** Arrows will mark printing direction, and the figures presented are not from Bjørheim’s testing but from optical light microscope pictures produced in this paper, as presented in chapter 5.3.

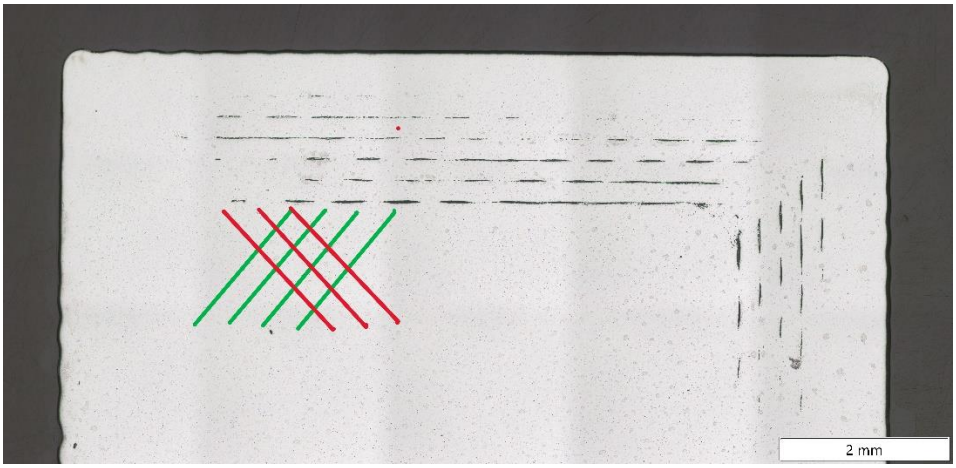

Fig 5 Longitudinal defects between each printing line

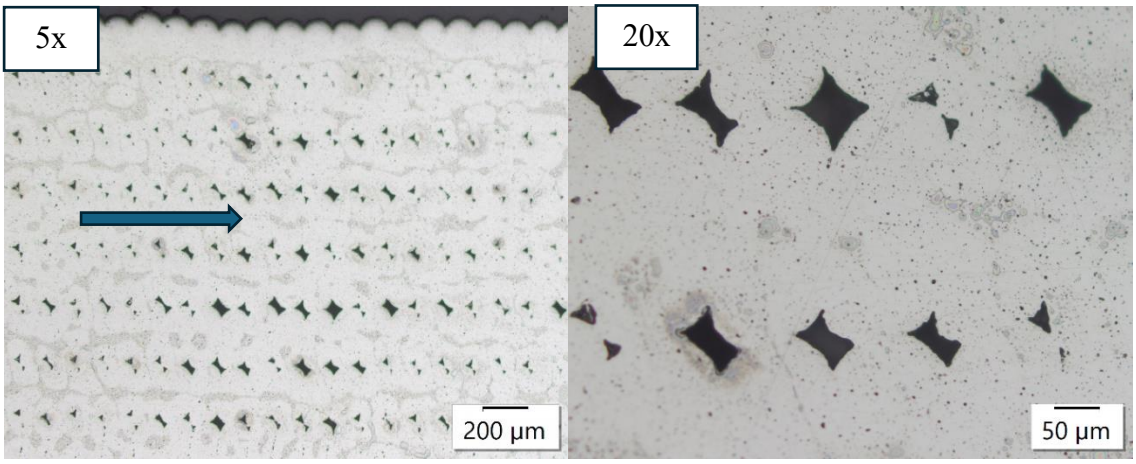

Fig 6 Cross-section of square defects

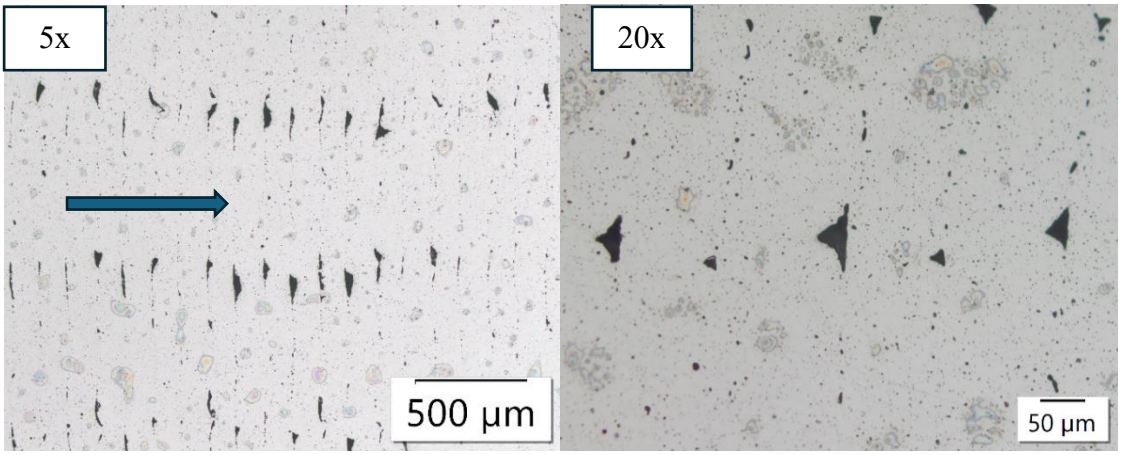

Fig 7 Cross-section of triangular defects

Gabilondo [35] found the same defects from printing as Bjørheim, and she also found a difference in how much of the cross-section consisted of pores. Her testing included the defects in the cross-section, and she found more pores and defects in the specimens consisting of only parallel printing lines as found in the wall section than in the specimen with solid infill.

Another possible defect found by Gabilondo [35] was cracks on the surface between layers. She found that when many pieces were printed at the same time, the printer would print some of one part, then print the same layers on another part before returning to finish the part it started printing. This means that the top layer has time to cool down before printing continues, possibly leading to poor adhesion. The cracks could be seen after sintering and may result from shrinkage and thermal gradients during sintering. Interestingly, the cracks only occurred in parts printed vertically, which can be due to the higher stress along the length of the

specimens, which is perpendicular to the printing direction for vertically printed specimens [35].

Tensile Testing

The tensile capacity of BMD printed parts depends on the printing direction relative to the applied tension, as found by Bjørheim and Lopez [3]. By producing and testing parts with three different printing orientations, it was clear that the capacity was different on all three parts. One of the parts, XY-flat, was printed flat, the next part, XY-sided, was printed on the side, and the last part, ZX, was printed vertically. Each part had three identical test specimens printed in 17-4 PH stainless steel.

When comparing the results, there was a clear correlation between the defects found in the microstructure and the results from the tensile test. The testing showed that the XY-flat specimens had the best mechanical properties and were the only results comparable to the mechanical properties stated by Markforged for 17-4 PH stainless steel. XY-flat had longitudinal defects parallel with the applied tensile force. The XY-sided specimen failed in the shoulder, and in the shoulder of said specimen, the longitudinal defects were perpendicular to the applied tensile force. This indicates that force applied at an angle to the defect can significantly reduce mechanical properties. The ZX specimen with even more defects perpendicular to the applied force failed in the gauge length at even lower stress than the XY-sided specimen [3]. Similar results were found by Henry [28] who tested specimens printed using only walls, both horizontally and vertically printed. He found that horizontally printed specimens showed significantly stronger ultimate tensile strength and yield strength.

When force was applied parallel with the longitudinal defects, Fig 8 shows the direction of the defects relative to the applied force, which is represented with an arrow. In Fig 9**,** the same can be seen for the force applied at an angle to the defect and in Fig 10 for the force applied perpendicular to the defect.

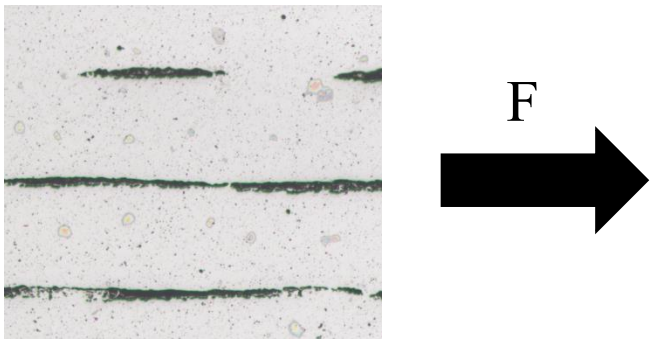

Fig 8 Force applied parallel with longitudinal defects

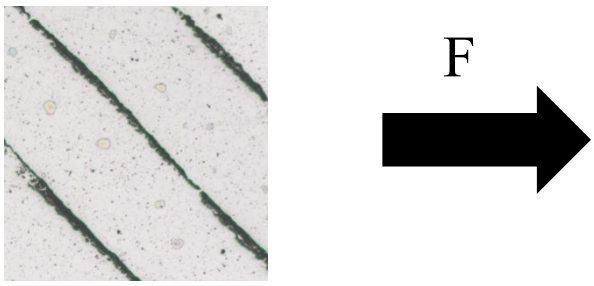

Fig 9 Force applied at an angle to longitudinal defects

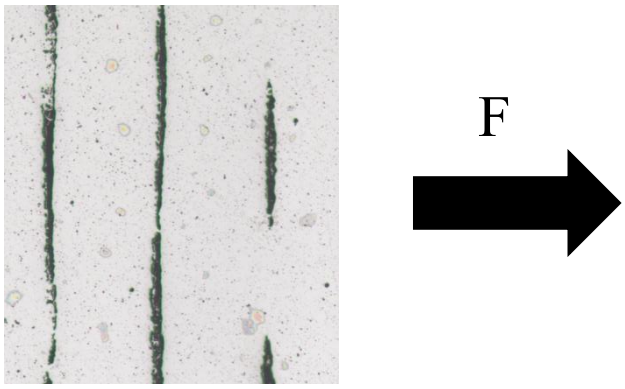

Fig 10 Force applied perpendicular to longitudinal defects

Lawrence [36] tested BMD specimens printed with solid infill as well as triangular infill. He found that the solid infill specimen's UTS was similar to its wrought counterpart, whereas the UTS of the triangular infill specimen was significantly lower. However, when normalizing the results by mass, he found that all three specimens had similar UTS. The wrought specimen showed the highest strain to failure, and the triangular infill specimen had the lowest strain to failure. Bradley [36] printed all specimens flat, with the walls and the parallel defects parallel to the applied force.

Fatigue Testing

Lawrence [36] tested cylindrical dog bones based on the ASTM standard E8 [37] that were modified to fit the tension-tension fatigue test fixture available to the authors, and printing was done using the Markforged metal X printer. The printed 17-PH parts were printed flat with four walls, using both solid infill for one type of specimen and triangular infill for another. A cold-drawn 17.46mm diameter round stock of 17-4PH stainless steel was used for the wrought specimens, and no heat treatment was applied. At least twenty specimens were made of each type.

Testing was conducted using the MTS Systems 810 servo-hydraulic load frame, and fatigue tests were performed using a frequency of 100 Hz and a stress ratio of R=0.1. Fig 11 shows that wrought-produced parts had a much higher fatigue capacity than that of their AM counterparts. Fig 12 shows that when the fatigue performance of triangular and solid infill specimens is normalized by mass, the fatigue capacity of the BMD parts is almost identical but still far below the fatigue capacity of the wrought parts. This can be a sign that defects affect the fatigue capacity in the AM parts that are not present in the wrought parts.

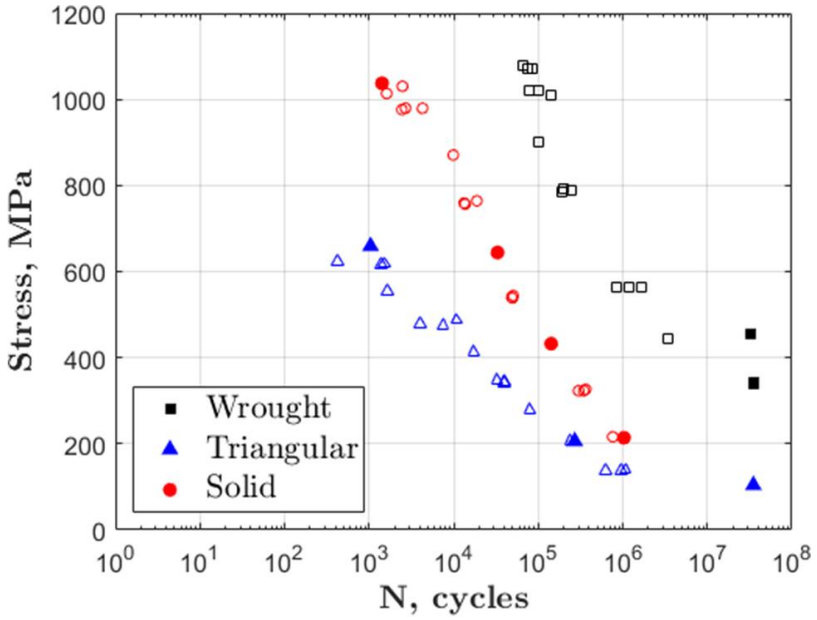

Fig 11 SN-Curve 17-4PH [27]

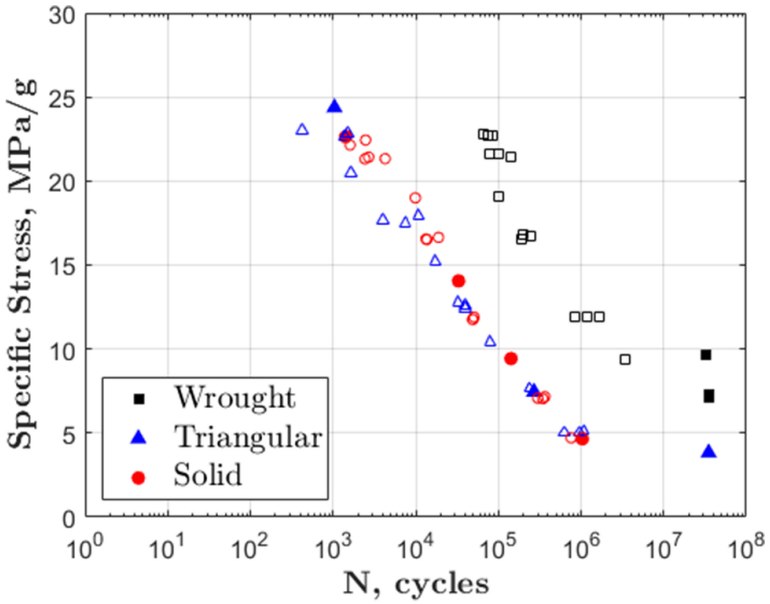

Fig 12 SN-Curve 17-4PH Mass Normalized [27]

Vickers Hardness Testing

Gabilondo [35] tested three specimens with five micro indentations each. The three specimens were printed horizontally and vertically, with one horizontal specimen consisting of only walls and the other having solid infill in addition to walls. The average hardness showed no significant difference between the specimens, showing that the printing direction should not affect the hardness of BMD specimens. When compared to Vickers hardness testing done by Bartolomeu [38] on the casted specimen and PBF specimen, the hardness was lower for the BMD specimen. The hardness of the specimen. was approximately 120HV for BMD, 230-280HV for cast, and 165HV for PBF. This shows that the hardness of BMD may be inferior to PBF. However, the hardness is known to be highly affected by the rate of cool-down, which is exceedingly long for the BMD part. The parameters for printing of BMD can be changed to allow for a quicker cooldown after sintering to improve hardness [38].

Post-Processing

Opoz [39] tested as-built, machined, and heat-treated specimens. He found that machining the rough surface significantly improved UTS, especially for parts printed at 30 and 60 degrees, which shows that machining can be used to make parts more isotropic. Furthermore, he found that heat treatment also enhanced UTS and that a combination of machining and heat treatment produced even better UTS. In addition to testing performed by Opoz, Bouaziz [40] found the same effect of heat treatment, with UTS improving significantly after heat treatment.

3. Theory

3.1. Fatigue Failure

Fatigue failure is when a part fails due to cyclic loading of tension or both tension and compression over time. Offshore structures, bridges, and mechanical equipment will often be subjected to cyclic loading from, among others, wind, waves, or vehicles. Fatigue can be divided into two major categories: high and low-cycle fatigue. High cycle fatigue is often related to linear elastic damage behavior with the number of cycles to failure above N = 10^4. Low cycle fatigue will typically be below N = 10^4 cycles and is related to plastic deformations accumulating until fracture [41]. High Cycle fatigue will be the focus area of this paper as high cycle fatigue testing was planned.

As explained by Larsen [41], a material's different stages when it fails due to fatigue are crack initiation, propagation, and ultimate failure. The initiation stage is when small deformation in local areas weakens the bonds between atoms, leading to small microcracks. Once the crack is initiated, plastic deformation will occur at the crack due to the stress concentration. Crack propagation is the stage where the crack grows due to the crack being opened for each cycle without closing, thus growing larger. Once a crack has been found, it is important to calculate how many load cycles it takes before the material reaches ultimate failure.

When evaluating fatigue capacity, locating places prone to crack initiation is important, as it is the first stage of fatigue failure. Crack initiation sites typically experience stress concentration, which is why it is critical for fatigue capacity. Stress concentration will typically form around holes or notches [42], which is why welds are especially prone to fatigue failure. Welds typically have defects such as micro cracks and pores, leading to a very short initiation stage[43]. Furthermore, experiments performed by Haldimann-sturm [44] found that the fatigue capacity of a common butt weld is usually weaker than the fatigue life of a casting node, with the results expected to be due to residual stresses and defects in the weld. Most AM methods will typically experience similar residual stress, micro-cracks, and pores as welding, which is why fatigue life is expected to be poor in AM parts [1].

3.2. 17-4 PH Stainless Steel

17-4 PH stainless steel is a martensitic precipitation hardening stainless steel used for industrial applications. The material is hard and provides high strength, outstanding wear

resistance, good toughness at temperatures up to 310 degrees Celsius, and moderate corrosion resistance [45]. Table I shows the mechanical properties of 17-4 PH stainless steel as sintered, and Table II shows the composition. Table I and Table II values are retrieved from Markforged [46].

Table I Mechanical Properties

Typical Mechanical Properties	**Test**	**Results**
Ultimate Tensile Strength	ASTM E8/E8M -22	1050 MPa
0.2% Yield Strength	ASTM E8/E8M -22	800 MPa
Young's modulus	ASTM E8/E8M -22	140 GPa
Elongation at break	ASTM E8/E8M -22	5 %

Table II Composition

Composition	**Weight %**
Chromium	15-17.5
Nickel	3-5
Copper	3-5
Silicon	1.0 Max
Manganese	1.0 Max
Niobium	0.15-0.45
Carbon	0.07
Phosphorous	0.04
Sulfur	0.03
Iron	balance

3.3. Tensile Testing Theory

Tensile testing determines mechanical properties such as ultimate tensile strength, yield strength, yield strain, ultimate strain, and ductility. Ultimate tensile strength is the highest

engineering stress a material can withstand. Yield strain is an elongation ratio at the point where the material starts to deform permanently, meaning that if the stress is released, it will not return to its original shape. Ultimate strain is an elongation ratio at the point of ultimate tensile strength. Ductility is a measurement of a material's ability to undergo significant plastic deformation and is an elongation ratio at the fracture point [47].

To calculate the elongation ratio, the following formula can be used:

$$\%El = \left[\frac{L_f - L_0}{L_0} \right] \times 100 \quad [47]$$

Where L_f represents the length of the material at the point of interest and L_0 represents the original length. Calculations for engineering stress can be found in Chapter 3.1.3.

The tensile testing process is as described by Davis [47]:

3.3.1. Test Specimen

A typical test specimen is shaped like a dog bone, as shown in Fig 13, and specifications for the geometry of the dog bone can be found in relevant standards**.** The specimens will have a gage area with a reduced cross-section relative to the grip section of the specimen to ensure that deformation and failure will happen in this region. It is also important that the grip section does not slip or fail before the specimen fails in the gage area. The cross-section can be cylindrical, square, or other shapes, and they should be designed following a standard for tensile testing to ensure that the geometry of the test specimen doesn't affect the results. If a standard has been followed, comparing results with other testing is reasonable. In contrast, where a specimen does not meet the requirements of a standard, deviations should be considered.

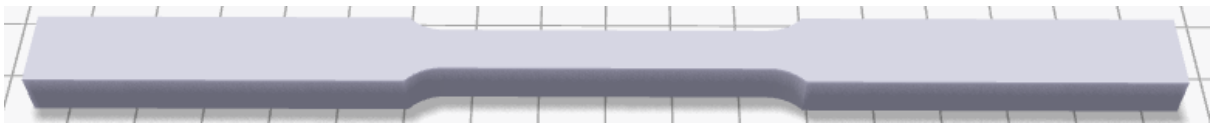

Fig 13 Typical test specimen

3.3.2. Testing Machines

The machine used for tensile testing is typically a universal tester that can test tension, compression, or bending. A testing machine is either electromechanical or hydraulic, with the main difference being the method by which the load is applied. An electromechanical machine has a wider range of test speeds and longer crosshead displacement, whereas hydraulic machines are more cost-effective in producing higher forces. Depending on the specimen's shape used for testing, there are a wide range of grips to hold the specimen in place. An example of a tensile testing machine is the Instron 5895 tensile testing machine, as seen in Fig 14.

Fig 14 The Instron 5895 tensile testing machine

3.3.3. Stress-Strain Curve

Engineering stress-strain curves are the relation between engineering stress and engineering strain. The engineering stress is defined as:

$$S = {}^{F}/_{A_0}$$

F is the applied tensile force from the machine, and A_0 is the initial cross-sectional area of the gage section.

Engineering strain(e) is defined as:

$$e = {\Delta L}/{L_0}$$

ΔL is the change in gauge length from before and after the tensile test. L_0 is the initial gauge length.

The advantage of comparing stress with strain is that they are independent of the cross-sectional area of the test specimen. It is important to note the difference between true stress and engineering stress. True stress is the actual stress on a material considering the instantaneous cross-section. In other words, it is the force applied, divided by the current cross-sectional area, while engineering stress is the applied force divided by the original cross-section. The stress-strain curve from the results of testing done for this thesis is presented in Chapter 5 in Fig 33**.**

3.4. High Cycle Fatigue Testing Theory

Fatigue testing can be done with the specimen subjected to only tensile force, compression force, or both tension and compression. The relationship between the minimum and maximum stress applied is denoted as the letter R. These are the ranges for R ratios for testing done only in tension, only in compression, or in both, as presented by Larsen [41]:

Only Tension: $0 \leq R < 1$

Only Compression: $1 \leq R$, or $R = \infty$

Both Compression and tension: $R < 0$

R is expressed as:

$$R = \frac{\sigma_{min}}{\sigma_{max}} \text{ [41]}$$

3.4.1. Test Specimen

As for tensile test specimens, the cross-section can be cylindrical, square, or other shapes, and they should be designed following a standard for fatigue testing to ensure that the geometry of the test specimen doesn't affect the results. If a standard has been followed, it is reasonable to compare results with other testing, whereas where a specimen does not meet the requirements of a standard, deviations should be considered. In fatigue testing, it is especially important to consider stress concentration in the specimen design. This is why a fatigue specimen typically

has a larger radius in the transition from the grip section to the gauge section, as seen in Fig 15.

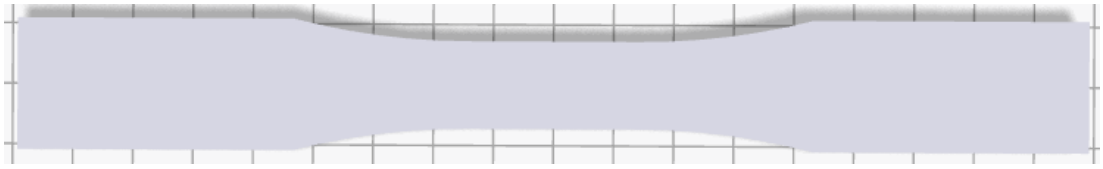

Fig 15 Fatigue Specimen

3.4.2. Testing Machines

Different test machines can be used, but they need to be able to generate the load amplitudes required for high-cycle fatigue [48]. The load frame includes servo-hydraulic, servo-electric, or linear-electric load frames with different force capacities and dynamic performance, and it is used to measure the force applied to the test specimen [49]. Fatigue testing differs in nature from tension testing in that the machine will apply cyclic loading instead of measuring the load applied before the specimen failed. An example of a fatigue testing machine is the 809 Axial/Torsional Test System, as seen in Fig 16**.**

Fig 16 809 Axial/Torsional Test System

3.4.3. SN-curve

An important outcome of fatigue testing is the SN-curve. To create an SN-curve, it is necessary to run several fatigue tests on the same material using different stress ranges, with the stress range being the lowest to highest stress applied for each cycle. It is also possible to run cyclic loading with different amplitudes, which is a separate way of defining cyclic loading. From the results obtained, curve fitting can be used to obtain an SN-curve. An example of an SN-curve can be seen in Chapter 2.5.2 Fig 11.

4. Experimental Details

The goal of the testing done in this paper was to investigate further the mechanical properties of 17-4 PH stainless steel when the specimens are printed using Bound Metal Deposition, with special attention given to the effect of the defects. Findings from Bjørheim's [3] testing was reviewed to determine design and printing directions for tensile and fatigue testing. Nine tensile tests were conducted with three different specimens. Fatigue testing was supposed to be conducted to find out if the fatigue capacity of BMD is anisotropic due to the longitudinal defects and to compare results with wrought specimens.

Two crucial issues arose that affected testing. The first was that the Markforged metal X printer at the University of Stavanger did not function, and with numerous unsuccessful attempts to resolve the issue, the parts had to be ordered from PLM Group, a partner of Markforged. This led to funding issues that meant not all parts could be ordered. The second issue was that fatigue testing could not be conducted as the machine did not function. Numerous unsuccessful attempts were made to resolve this issue, and it was evaluated if the tensile test machine could be used for fatigue testing. The machine was not suitable for fatigue testing, and therefore, fatigue testing could not be conducted. Instead, the effect of the longitudinal defects is thoroughly interpreted and discussed.

4.1. Part Production

The design of the parts was done in a CAD program before the drawings were exported as STL files to a Markforged software called Eiger. In this program, parameters such as printing orientation and number of walls were chosen before the specimens were ready to be printed. Before the printer started, Eiger, which is printing software, sliced the model into thin layers and gave the printer all the necessary information, such as the number of layers, thickness of each layer, printing speed, and temperature. All specimens were printed with 17-4 PH stainless steel, a post-sintered layer of 0.127mm, and solid infill.

The specimens were printed using the Metal X system from Markforged, as presented in Fig 17. The maximum build volume for this printer is:

Width: 300mm

Depth: 220mm

Height:180mm

The de-binding process was performed using Wash-1 from Markforged, as pictured in Fig 18**.** It has a maximum working volume of 356x254x203 mm.

Sinter-1 from Markforged was used for sintering the parts, as pictured in Fig 19. This sinter has a maximum sintering capacity of 305 mm and is cylindrical with a diameter of 141mm and a length of 305mm. The sinter chamber is pictured in Fig 20**.**

Fig 17 Markforged Metal X Printer

Fig 18 Markforged WASH-1

Fig 19 Sinter 1

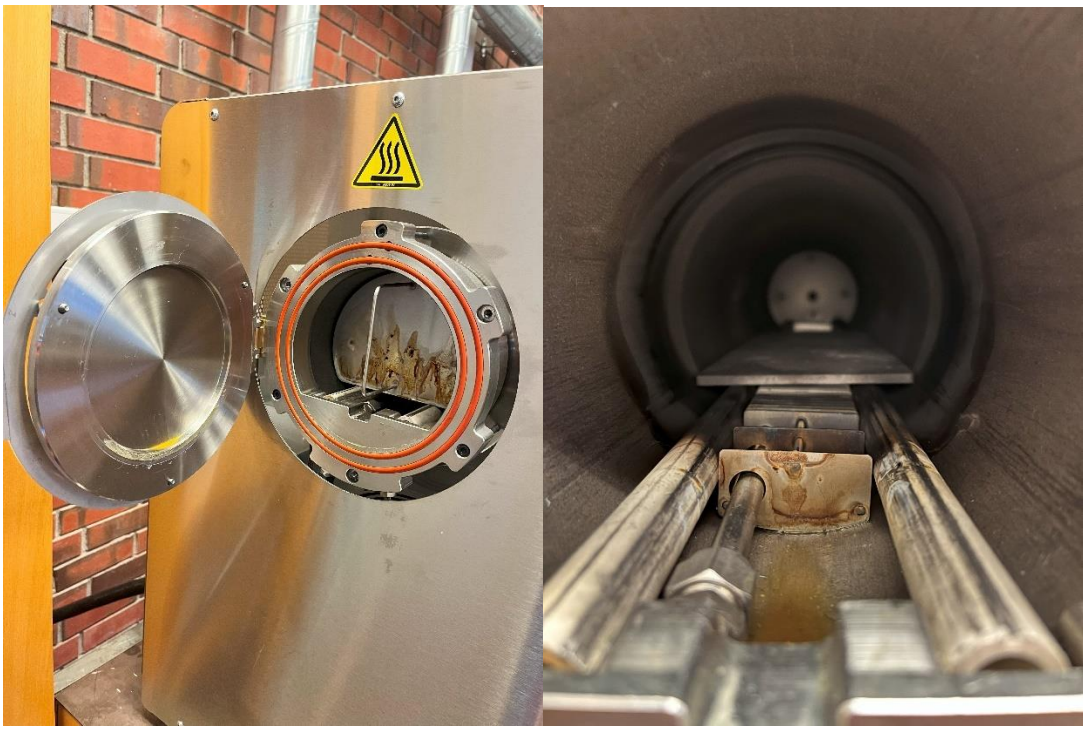

Fig 20 Sinter 1

4.2. Tensile Testing

For tensile testing, three parts were made of each specimen. The three different specimens were named XY-2, XY-Longitudinal, and XY-45, and specimens were designed following ASTM E8/E8M – 22 [37]**.** Tensile testing was performed at room temperature and monotonically loaded until failure, and ASTM control method c) crosshead speed was used. The machine utilized for the tensile testing was an Instron 5895 tensile testing machine with a 250kN loading cell**,** capable of measuring both deformation and applied load. All specimens were loaded to the point of fracture, and deformation was measured with the internal deformation measuring system. Results obtained from the testing were yield tensile strength (YTS), ultimate tensile strength (UTS), Young's modulus (E), and Elongation (%).

Specimen XY-2 was geometrically identical to the specimens Bjørheim made for his tensile testing [3], as seen in Fig 21, but the difference was that Bjørheim's test specimens had eight walls, while XY-2 had two. The goal was to see if there was any correlation between the number of walls and the tension capacity. As specimen XY-2 has more longitudinal defects at an angle to the applied tensile force, XY-2 is expected to be weaker than specimen XY-flat from Bjørheim's tensile testing. The digital printing pattern of the part is presented in Fig 23**.**

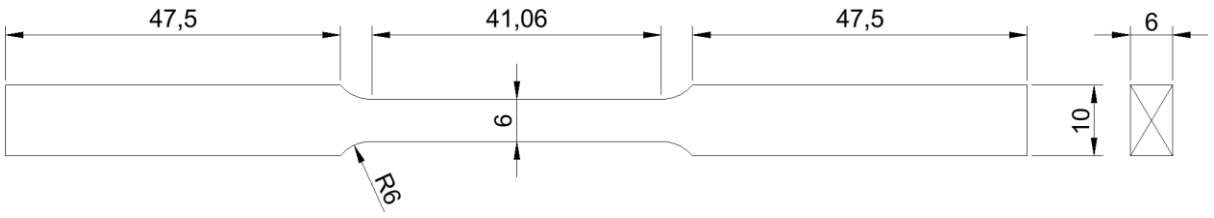

Fig 21 XY-2 Geometry

Specimen XY-Longitudinal was designed with a gauge area consisting of only walls, as presented in Fig 24. The objective of testing this specimen was to find the mechanical properties of the material when the force is solely pulling parallel to the longitudinal defect.

Specimen XY-45 was printed larger than the XY-Longitudinal specimen so that when two walls were chosen in Eiger, the geometry of the fill-in part was identical to the outer geometry of the XY-Longitudinal specimen. Specimen XY-45 was machined to achieve this, and the gauge section of the part was then made of only fill-in, which means the gauge section had longitudinal defects at an angle to the applied force. The printing pattern for XY-45 is presented in Fig 25, with an orange arrow marking the width that is identical for specimens XY-longitudinal and XY-45. The initial test-ready geometry of XY-longitudinal and XY-45 is presented in Fig 22**.** Due to machining limitations, the grip section of XY-45 is wider, but the gauge section and radius of the transition from gauge to grip section are identical.

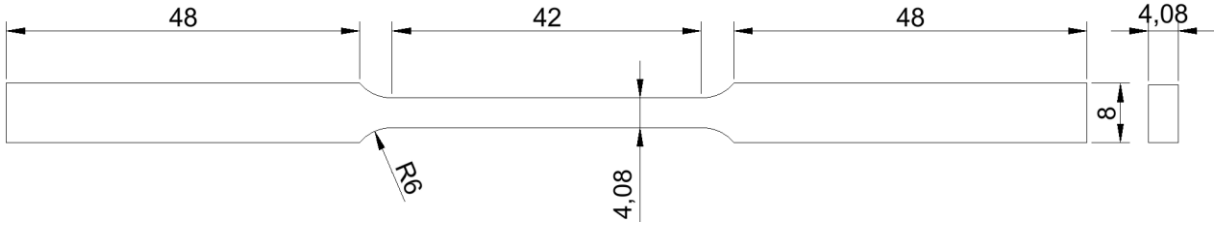

Fig 22 XY-Longitudinal & XY-45

The reason for testing specimens XY-45 and XY-Longitudinal is to have even more data regarding the effect of the defects. As the 45-degree infill has more longitudinal defects at an angle to the applied tensile force, XY-45 is expected to have a lower tensile capacity than specimen XY-Longitudinal. Performing these tests will also show if the fill-in or the walls of BMD parts have better mechanical properties.

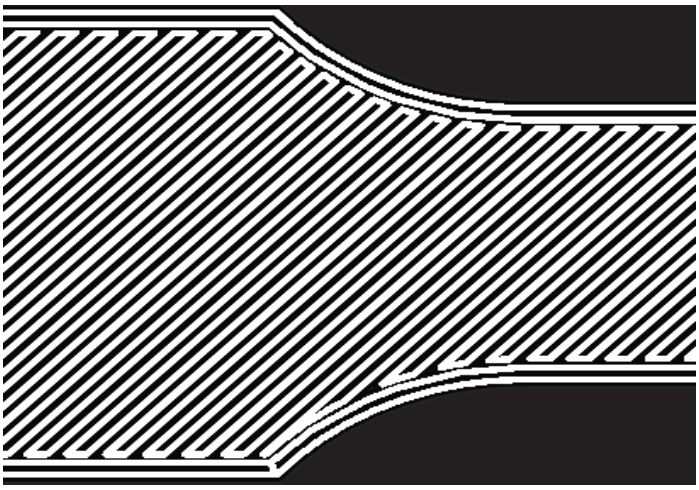

Fig 23 XY-2 Printing Pattern

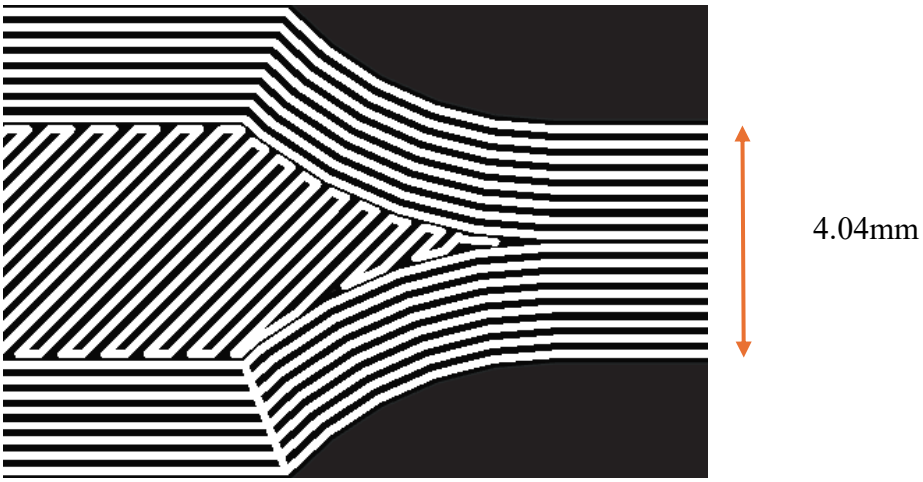

Fig 24 XY-Longitudinal Printing Pattern

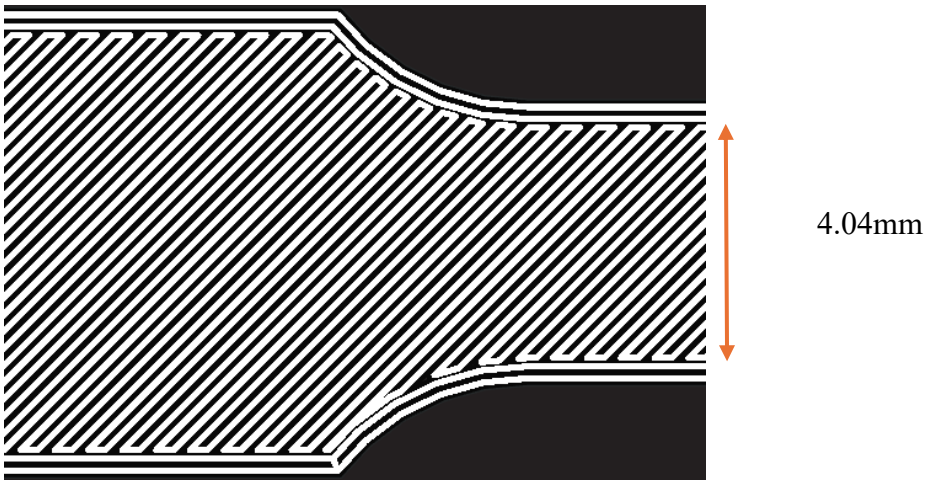

Fig 25 XY-45 Printing Pattern

4.3. High Cycle Fatigue Testing

Five identical parts of specimen XY were printed horizontally for fatigue testing. All parts were made following ASTM E466:21 [50]. An attempt was made to print vertical specimens (ZX) to compare them with the horizontally printed specimens, but due to unforeseen circumstances, these specimens were not printed. Fatigue testing was to be performed on an 809 Axial/Torsional Test System with a 647 hydraulic wedge grip, with a frequency of 15 Hz and the stress ratio at R=0.1.

In the test specimens used by Lawrence [36] the transition section had defects perpendicular to the applied tensile force because of their cylindrical shape. Bjørheim [3] found that specimens with longitudinal defects perpendicular to the applied tensile force are detrimental to fatigue capacity, and his tensile testing found that the specimens with such defects in the transition section all fractured in this section. Therefore, flat specimens were designed for the tests, as presented in Fig 28**.**

Fig 27 shows specimen XY as seen from above, and Fig 28 is the same specimen but further zoomed in**.** Fig 29 illustrates how the vertically printed specimen would look, as seen from above, and Fig 30 shows a 3D view of this specimen. The figures can be used to understand the direction of the defects, as each layer will look the same as the figures illustrate, only with the infill iteratively changing direction layer by layer. The geometry for the specimens is presented in Fig 26.

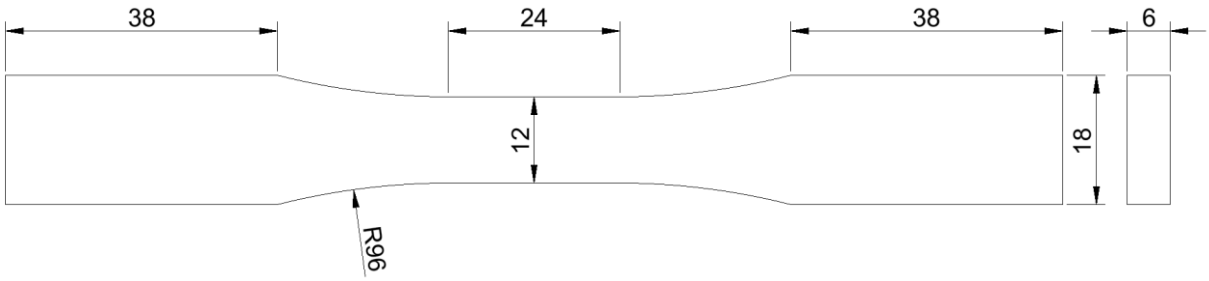

Fig 26 XY Geometry

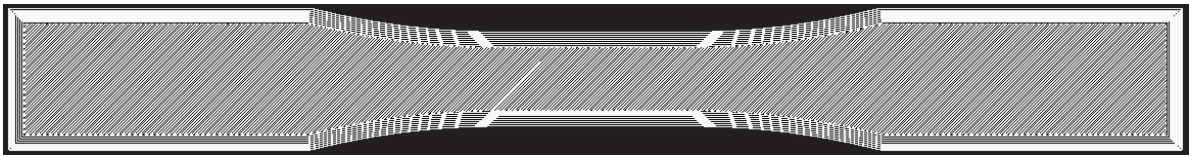

Fig 27 XY Printing Pattern

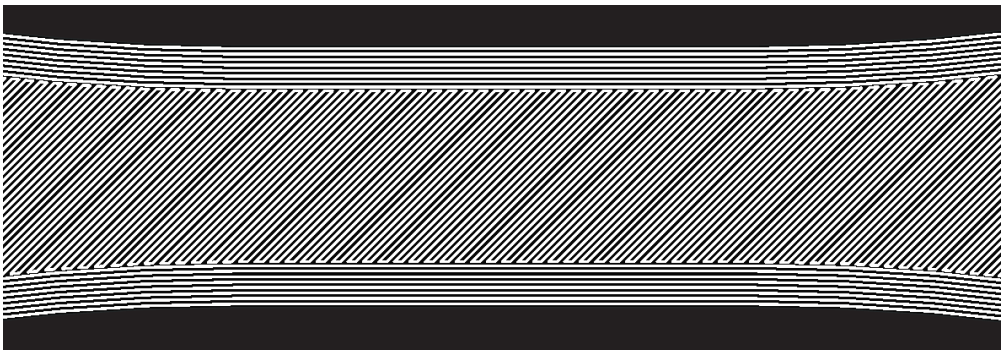

Fig 28 XY Printing Pattern Zoom

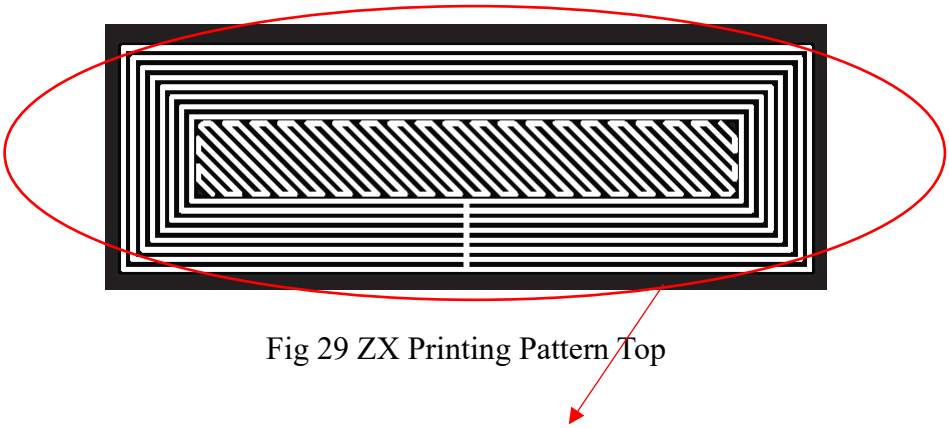

Fig 29 ZX Printing Pattern Top

Fig 30 ZX

4.4. Optical Light Microscopy

For the optical light microscopy (OLM), a box was printed vertically, and test specimens were cut using a Discotom-10 cutoff machine operated at a feed speed of 0.25mm/s. The original shape of the box is illustrated in Fig 31**,** and the parts cut to use for OLM are illustrated in the same figure as part 1 and part 2. Part 1, cut to 10mm length and 10mm width, will show the longitudinal defects, whilst part 2, cut to 10mm length and 10 mm width, will show the cross-section of the defects. Fig 32 illustrates the printing pattern as seen from above.

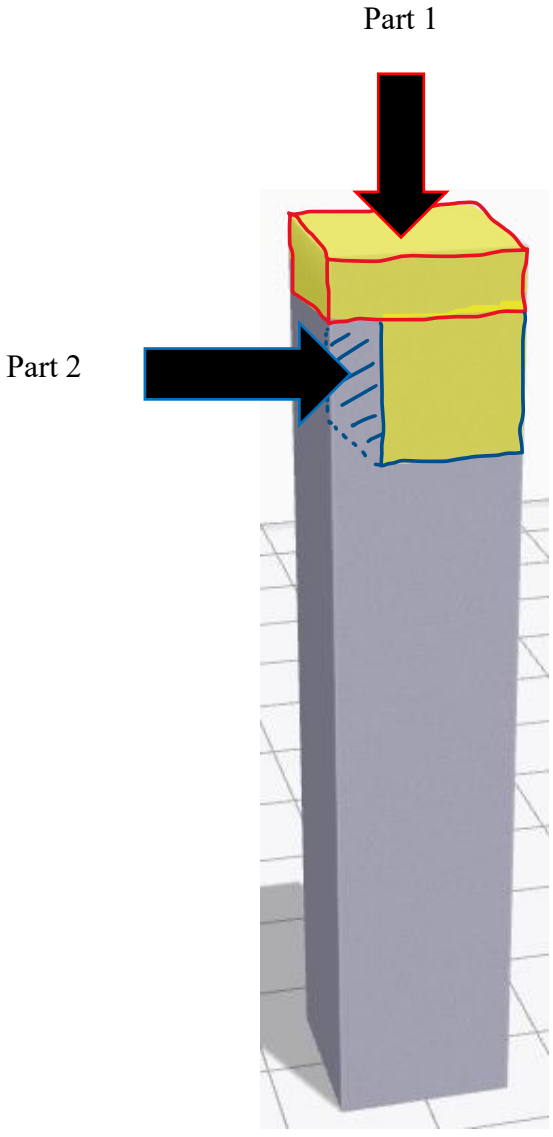

Fig 31 BOX

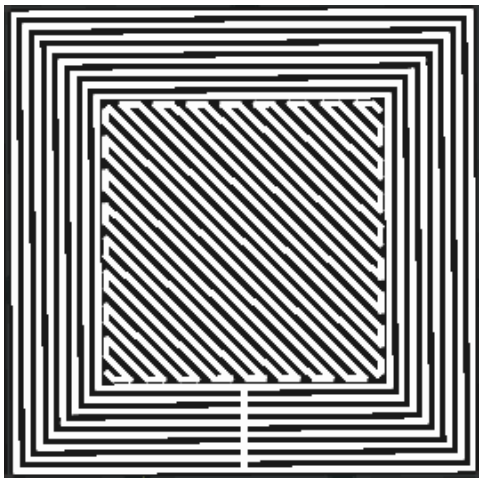

Fig 32 printing pattern

After the parts were cut, they were molded in epoxy using a Struers Citopress-30 mounting press before being mounted in a cylinder with a diameter of 25mm using electrical leading acryl (ConduFast). The bottom was made with transparent acrylic resin (ClaroFast) to work as a surface electric insulator for ConduFast. The parts were marked and then ground as well as polished using a Struers Tegraforce-5 using the following steps:

- MD-Piano 220 grit ground for 2 minutes with water coolant.
- MD-Allergo, DiaPro AllegroLargo 9 μm, polished for 3 minutes.
- MD-Dac, DiaPro Dac 3 μm polished for 4 minutes.
- MD-Dur, Nap-B 1 μm polished for 4 minutes.

The objective of performing optical light microscopy was to confirm the presence of defects and to have pictures to better illustrate the effect of the defects.

5. Results And Discussion

5.1. Tension Testing Results

Results from testing of BMD-produced specimens can be seen in Table III**,** With specimen "Markforged As-sintered" representing the as-sintered mechanical properties of 17-4PH stainless steel when printed using BMD, as presented by Markforged [46].

Table III Tension Testing Results

Specimen	**Yield Strength (MPa)**	**Ultimate Tensile Strength (MPa)**	**Young's Modulus (GPa)**	**Elongation at Break (%)**
Markforged As sintered	800	1050	140	5
XY-2 1.	580.9	1066.2	55.86	7.1
XY-2 2.	560.4	1058.6	57.49	7.2
XY-2 3.	523.3	1058.0	56.37	7.3
XY-Longitudinal 1.	357.7	1040.1	26.83	9.8
XY-Longitudinal 2.	395.6	1033.1	26.12	8.8
XY-Longitudinal 3.	356.8	1029	28.01	9.4
XY-45 1.	338.4	1095.9	27.78	8.8
XY-45 2.	362.8	1089.4	33.46	8.5
XY-45 3.	369	1103.5	30.05	9.0

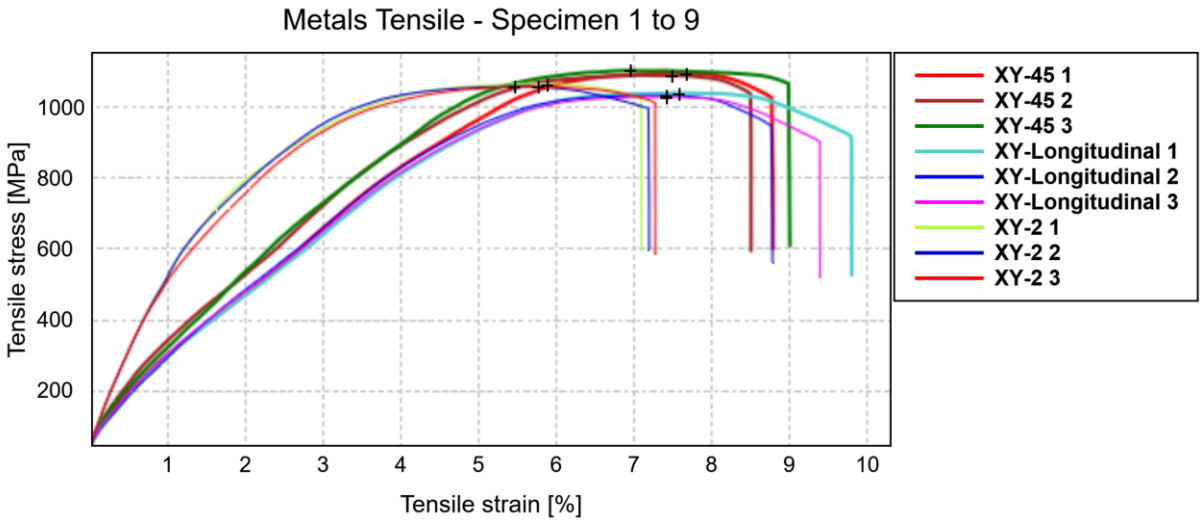

Fig 33 Engineering stress-strain curve of all tensile tested 17-4 PH stainless steel specimens

The tensile force was applied until fracture on all nine specimens, and they all fractured in the gauge area, as presented in Fig 36. The values for Yield strength, Young's modulus, and elongation appear to be inaccurate as the yield point on the graph looked to be much higher than what was read by the machine, and elongation is higher than previous testing. This is expected to be the result of inaccurate measuring of deformation by the Instron 5895 tensile testing machine. Ultimate tensile strength and elongation at break will be the only values used to compare the specimens. The results for ultimate tensile strength are not dependent on measuring deformation, meaning the results are dependable when compared with other tests. Elongation can still be used to compare the specimens in this test, but it is not accurate enough to compare with other testing methods.

Specimen XY-2 presented, on average, 7MPa lower UTS than the part previously tested by F. Bjørheim that had eight walls, which is well within normal deviations. This shows that the number of walls has almost no impact on the mechanical properties of the specimen, and XY-2 showed higher UTS than the values given by Markforged, showing that printed parts are not necessarily dependent on having eight walls to reach the mechanical properties given by Markforged.

Specimen XY-45 appears to have an average of 62,2Mpa higher ultimate tensile strength than XY-Longitudinal, and this is different than what was expected due to the defects. A reason for XY-45 to have a higher tensile strength can be that the cross-section has less missing material from the defects, giving it a slightly higher effective area than the cross-section of XY-

Longitudinal. This is due to the defects in the XY-45 gauge section having a triangular shape, whereas the defects in the gauge section of XY-Longitudinal have a square shape. In addition, the distance between the defects is also longer in XY-45. Measuring defects were performed, and new UTS results using the calculated effective area of specimen XY-45 and XY-Longitudinal are presented in Chapter 5.2.

Another reason for the XY-45 specimen having a higher UTS is that in specimen XY-45, the gauge section had to be machined, giving it a better surface area. The surface area of specimen XY-Longitudinal, as sintered, has a rough surface where stress concentrations can occur, but as the printing direction is parallel with the direction of applied force, the roughness is not expected to affect the results significantly. Overall, the ultimate tensile strength of XY-45 was above the values given by Markforged, whereas XY-Longitudinal was slightly below the given values.

Specimen XY-Longitudinal had a higher percentage of elongation than XY-45, showing that the walls of the print have a more ductile behavior when pulled parallel to the printing direction than the solid infill. The XY-Longitudinal specimens had clear necking before fracture, whereas XY-45 barely had necking, which is another sign of a more ductile behavior of XY-Longitudinal.

The ductile behavior of XY-Longitudinal can be explained by the longitudinal defects as well as the printing direction being parallel with the applied tensile force, meaning that all deformation happens in the direction of the force applied, as presented in Fig 34. This is not the case for XY-45 as the printing is done with a 45-degree angle to the applied force, and each layer changing direction creates a mesh of defects, as illustrated in Fig 35. The defects decrease the contact between each printing line, allowing them to elongate separately to a certain degree. Each of these “strings” deforms, but they are shorter than the “strings” that appear in XY-Longitudinal and cannot elongate as freely as they are held together in a mesh, leading to specimen XY-45 having less elongation. This printing geometry can also affect the tensile strength because it makes it harder for dislocations to migrate through the material.

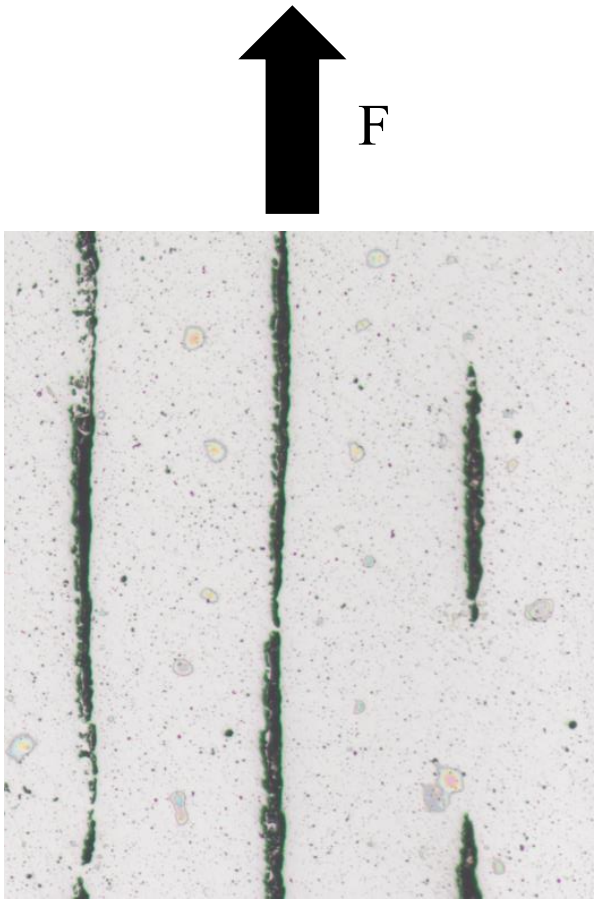

Fig 34 Defects in the gauge section of XY-Longitudinal

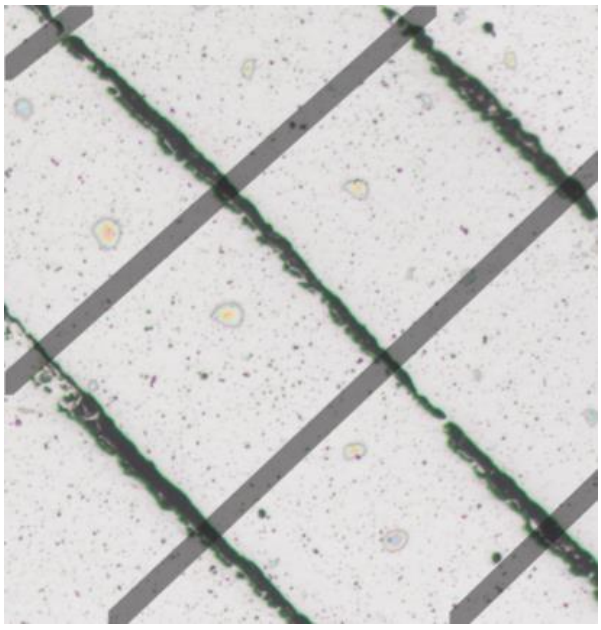

Fig 35 Illustration of a mesh of defects in the gauge section of XY-45

Below is a picture of all the parts after tensile testing. The specimen lay in the following orientation from the left in groups of three of each specimen: XY-2, XY-longitudinal, XY-45.

Fig 36 Fractured Specimens

5.2. Results with Adjusted Cross-Section Area

Two different methods were used to determine how much of the cross-section area was missing due to defects in the plane. An optical light microscope GX53 was used for the pictures, and a specimen different from the test specimens was used, but the defects are the same.

Results from the first method, using software to calculate, showed that in specimen XY-45, 1.75% of the cross-section area is missing due to defects, while in XY-Longitudinal, 4.13% is missing. Fig 37 and Fig 38 show the area used to calculate the percentage of missing cross-sectional area, and as can be seen, some imperfections other than the defects affect the results.

The second method used to find the total area of the defects was to measure several defects and calculate the average area per defect before multiplying by the number of defects in the cross-section of each tested specimen. Fig 39 shows an example of some of the measurements used for this method. The results were that 3.48% of the cross-section is missing in specimen XY-Longitudinal, and 2,11% is missing in specimen XY-45.

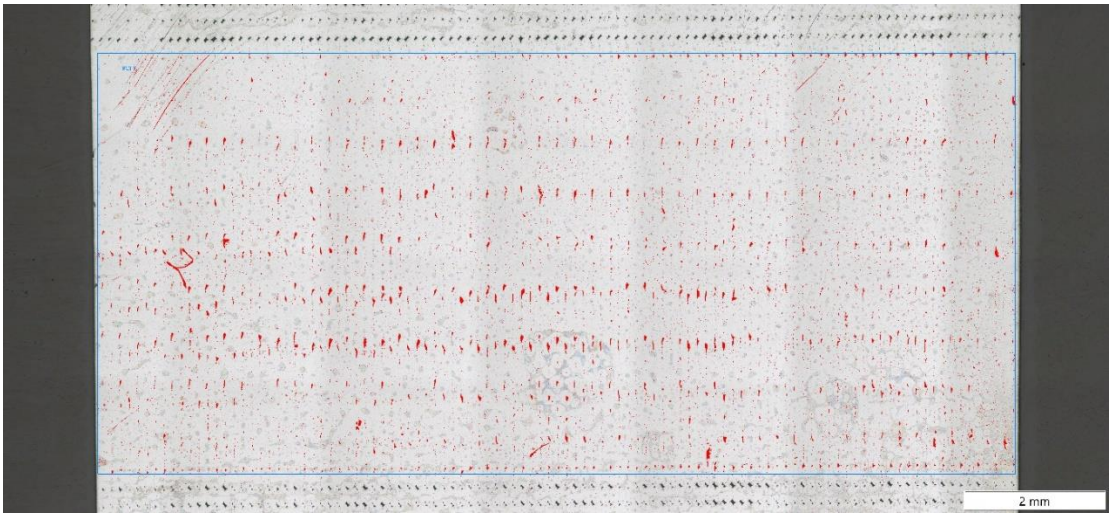

Fig 37 Cross-sectional defects of infill

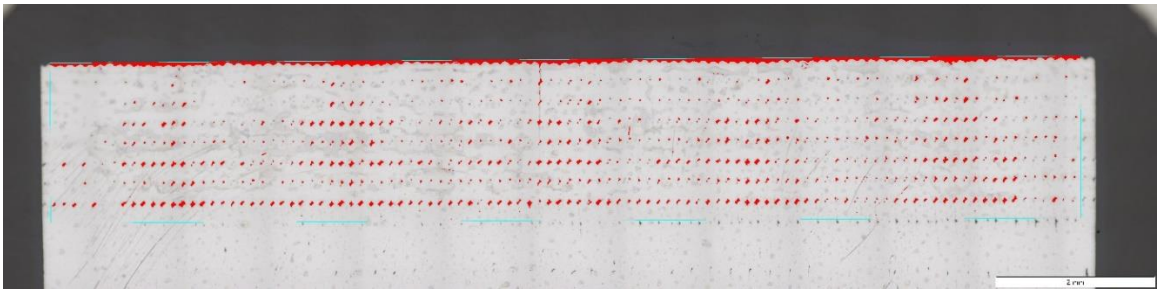

Fig 38 Cross-sectional defects of walls

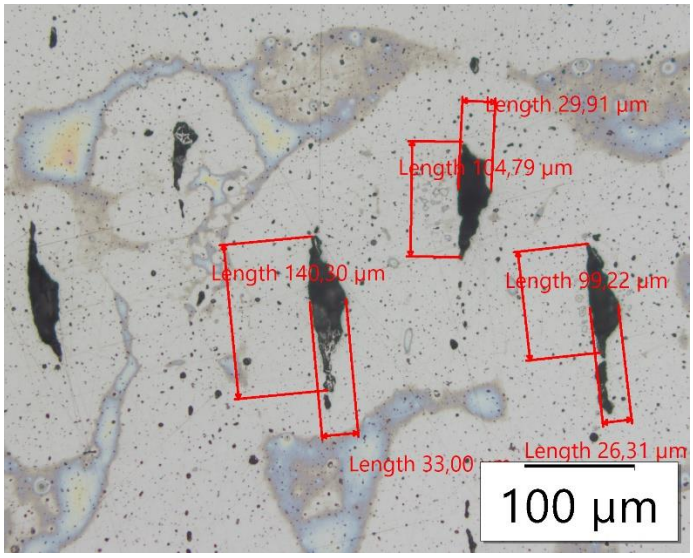

Fig 39 Measuring of defects in cross-section

The results showed that the difference in missing cross-section due to the defects is small in both methods, and the results from the first method were used to calculate the new net effective area of the two specimens because this method had the highest difference. Table IIII below presents the UTS of the specimen with the adjusted effective area (A_{net}) of the cross-section compared to the UTS using the original cross-section (A). In addition, a stress-strain curve using A_{net} is presented in Fig 40.

Table IIII Comparison of tensile specimens

Specimen	**Ultimate Tensile Strength (MPa)**	
	A	A_{net}
XY-Longitudinal 1.	1040.1	1083.1
XY-Longitudinal 2.	1033.1	1076.2
XY-Longitudinal 3.	1029	1071.3
XY-45 1.	1095.9	1114.9
XY-45 2.	1089.4	1108.1
XY-45 3.	1103.5	1122.6

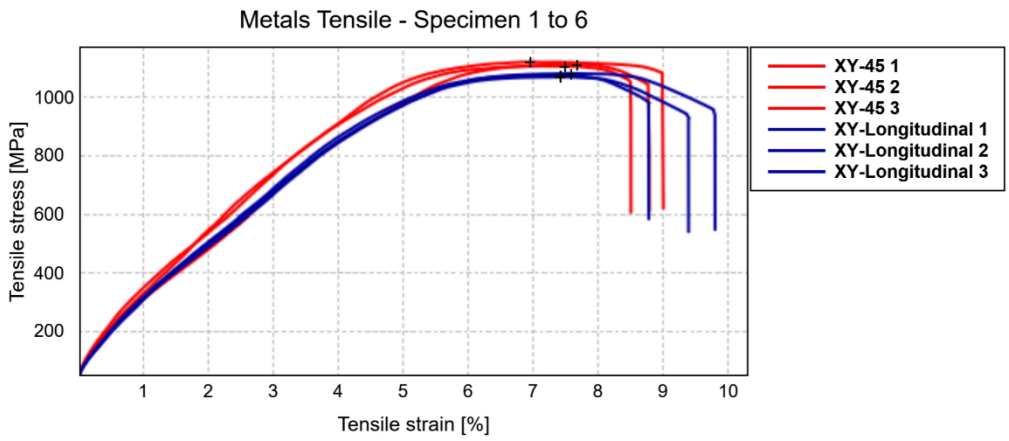

Fig 40 Graph of the tensile specimen with new effective cross-section

The average difference in tensile strength went from 62Mpa to 38Mpa, which is not a significant change. If A_{net} had been calculated using the second method, the change would have been even smaller. The effect of the defect on A_{net} may influence the mechanical properties but does not appear to be the only reason for the difference in UTS.

5.3. Optical Light Microscope Results

Figs 41**,** 42**,** 43, and 44 show pictures from the OLM. Fig 41 provides an overview of Part 1, and Fig 42 provides an overview of Part 2. Fig 43 shows defects in the walls of Part 1, while Fig 44 shows defects in the solid infill of Part 2.

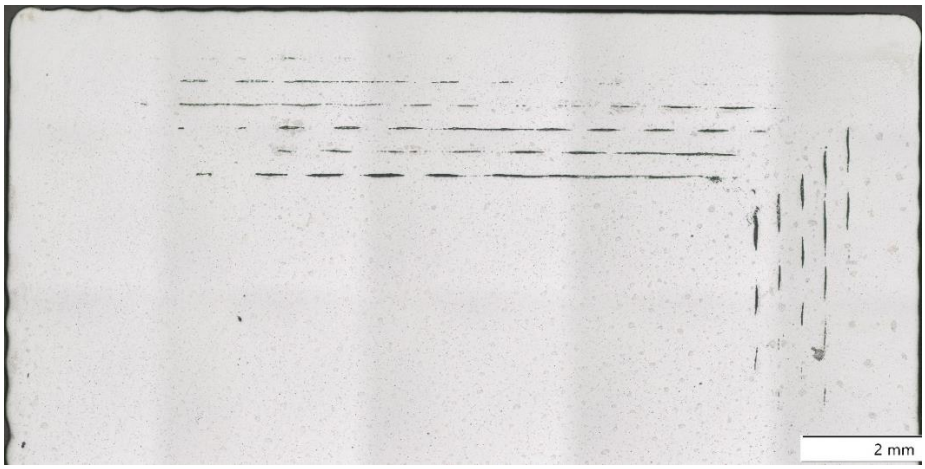

Fig 41 Part 1

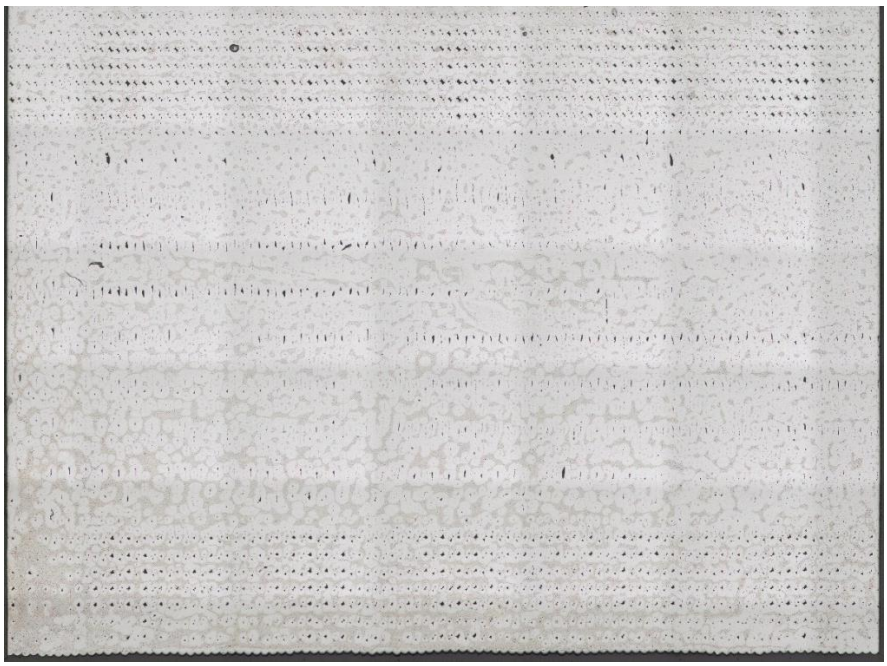

Fig 42 Part 2

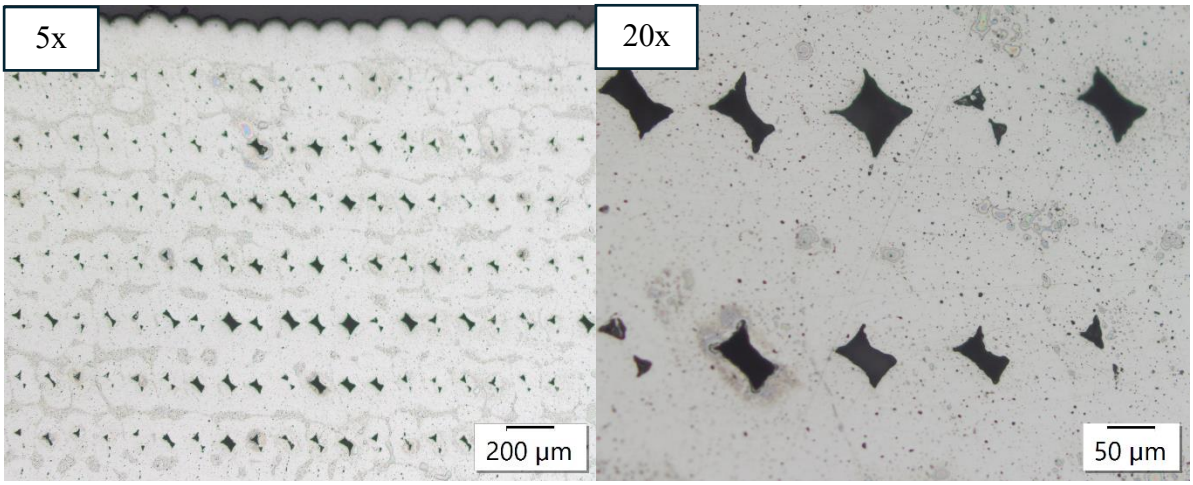

Fig 43 Defects in the wall section of the print – Part 2

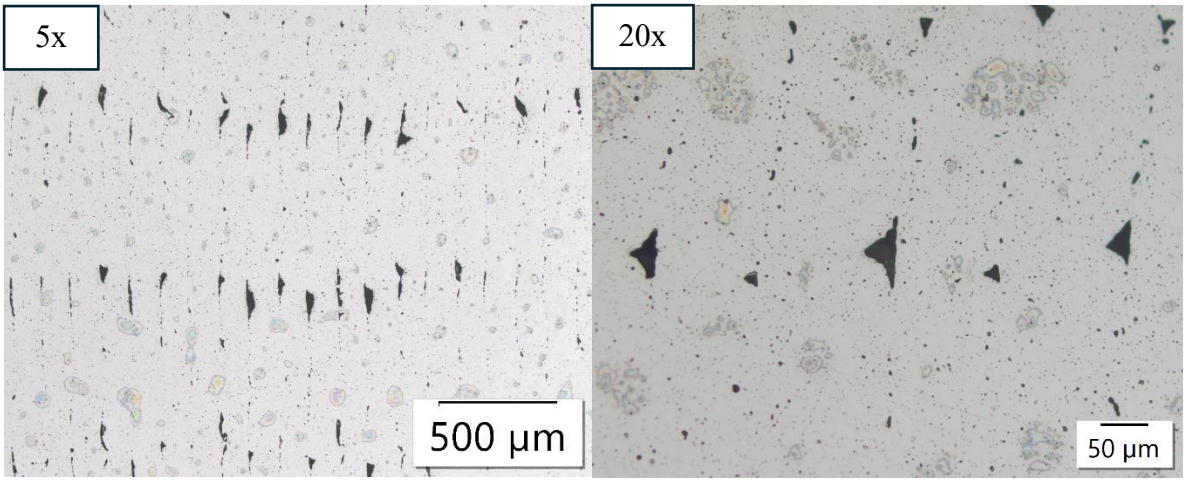

Fig 44 Defects in solid infill section – Part 2

The longitudinal defects in Part 1 are visible in the wall section, but the longitudinal defects expected to be in the solid infill part are not visible. However, the defects in Part 2 are clearly visible in both the wall section and the solid infill part. In addition to the defects following each printing line, visible pores are all over prints 1 and 2.

5.4. Fatigue Testing Results Discussion

Due to unforeseen circumstances, fatigue testing could not be performed. Instead, the following chapter will discuss plausible outcomes derived from tensile testing, previous fatigue testing, and interpretation of the effect of defects.

The results from Bjørheim's tensile testing showed that the horizontally printed specimens had significantly higher tensile capacity as well as ductility when compared to the vertically printed specimen [3]. Therefore, a horizontally printed specimen is expected to have a much higher fatigue capacity. The fatigue capacity of BMD parts is expected to be lower when compared to wrought specimens, as found by Lawrence [36].

The main reason for expecting the fatigue capacity of the vertically printed specimen to be lower than that of the horizontally printed specimen is that the longitudinal defects in the wall section will be perpendicular to the applied force. These defects' cross-sections can be seen as holes or existing cracks; whether they are cracks or not is highly debatable. Either way, the defects are holes prone to crack initiation due to stress concentrations, which means that the initiation stage is expected to be short or almost non-existent. As the initiation stage is usually a substantial part of reaching fatigue failure, a practically non-existent initiation stage is

critical. It is also normal for crack propagation to take time before the crack reaches a substantial length, but if cracks start forming between the defects, as presented in Fig 45, it should not take long before the crack is significant.

The rough edge of the BMD part is also prone to cracks being initiated due to stress concentrations. This means cracks can be formed between the defects or on the edge due to the rough surface, as presented in Fig 45. Either way, the ZX specimen is expected to fail in the wall section of the print, where the defects are seen as most critical.

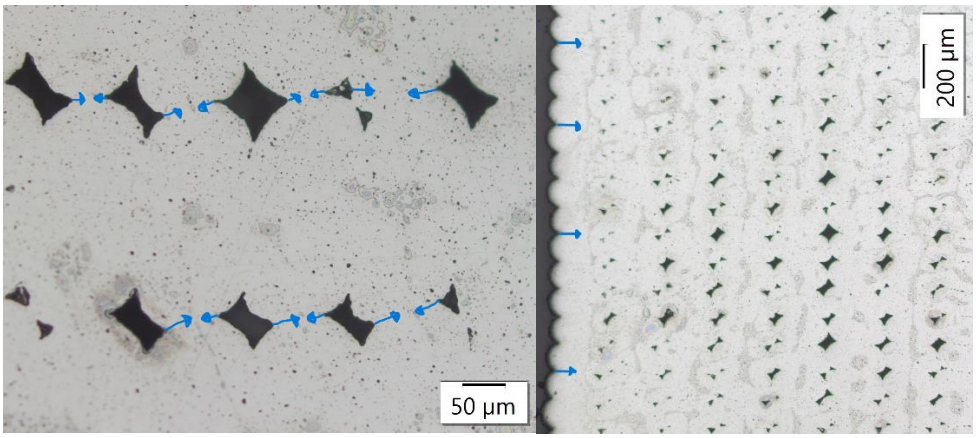

Fig 45 Crack Initiation and Propagation

The longitudinal defects in the walls of XY are parallel to the applied force, so the defects in the infill are expected to be more critical. The longitudinal defects in the infill part will be orientated at an angle relative to the applied force, as presented in Fig 46. This means that some of the force will create normal stress, and some will create shear stress, as shown by the red and green arrows in Fig 46. As a result, the stress contributing to the initiation and propagation of a crack between the defects differs from the stress in the vertically printed specimen, which should only experience normal stress.

Section A-A, marked in Fig 46, can be seen in Fig 47, which shows an illustration of the cross-section of the infill part together with blue arrows to show expected crack initiation sites. One way for the crack to propagate in the infill section is if a similar crack initiates in the layer above or below, leading the cracks to grow together, as marked by green in Fig 47. Another way a crack can be initiated in the infill part is along the longitudinal defect, which can also be initiated by shear and normal stress.

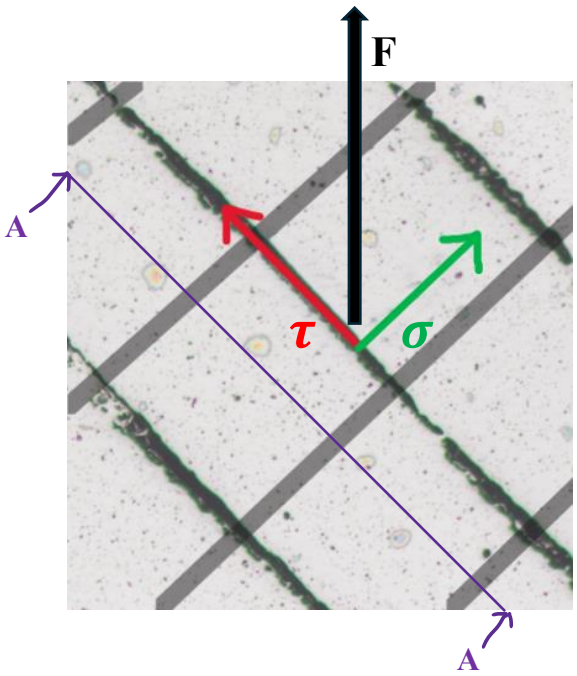

Fig 46 Stress distribution on defects in horizontally printed specimen XY

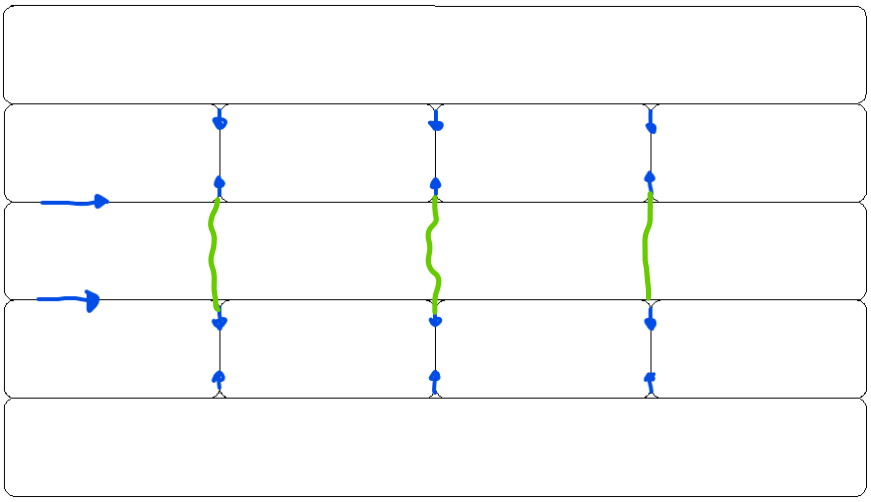

Fig 47 Section A-A crack initiation alternatives

In addition to the defects in the AM parts, there are also apparent pores that look to be following the printing direction, indicating that the pores are defects from the printing process. When there are pores between the defects where the crack is expected to initiate, the propagation stage can be shortened, and larger pores are also prone to crack initiation. Fig 48 shows the pores discussed above.

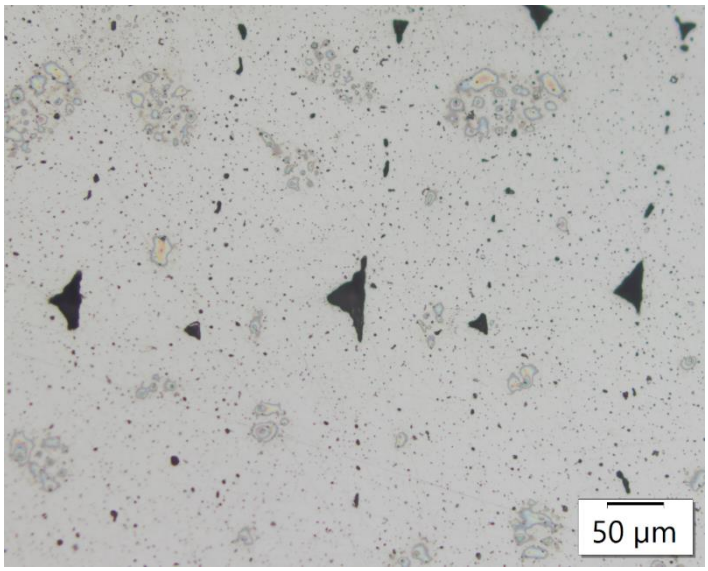

Fig 48 Pores in cross-section of infill part

6. Conclusions

The purpose of this thesis was mainly to find the effect of printing defects on the mechanical properties of BMD and to understand the effect of the defects on fatigue capacity. The following results were found:

- The orientation of longitudinal defects influences Bound Metal Deposition (BMD). Interestingly, the angle of these defects relative to the applied force significantly affects the mechanical properties. Previous testing in reviewed literature showed that vertically printed specimens had worse mechanical properties than horizontally printed specimens. Comparing specimen XY-45 and XY-longitudinal, it was found that specimen XY-45 with longitudinal defects at a 45-degree angle to the applied force, and the printing direction iteratively changing layer by layer was strongest. Specimen XY-longitudinal with all the longitudinal defects parallel to the applied force was more ductile
- The Literature review found that fatigue capacity in PBF and DED is adversely affected by pores, lack of fusion, and rough surfaces, all of which contribute to stress concentration. Residual stress in AM further diminishes fatigue life. Similarly, the defects in BMD and the rough surface of vertically printed specimens are prone to stress concentrations. Cracks are expected to initiate and propagate through the defects.
- Testing showed that the difference in using two or eight walls is within normal deviation, and both parts produced ultimate tensile strength results within the mechanical properties given by Markforged.

7. Future Research

Future research should study:

- The presence of pores and their effect on mechanical properties in BMD.
- The effect of cracks between printing layers on mechanical properties and how different printing parameters affect their occurrence.
- If residual stress can be found in BMD specimens, and what produces them.
- Fatigue testing, as presented in this thesis, and analysis of crack initiation to see if they follow the expected results or if new findings can be made.

References

[1] T. DebRoy *et al.*, “Additive manufacturing of metallic components – Process, structure and properties,” *Prog. Mater. Sci.*, vol. 92, pp. 112–224, 2018, doi: 10.1016/j.pmatsci.2017.10.001.

[2] T. Halvorsen and G. M. Lamvik, “Additive Manufacturing of Spare Parts in the Maritime Industry: Knowledge Gaps for Developing a Norwegian AM-Based Business Ecosystem for Maritime Spare Parts,” in *484-491*, A virtual conference hosted by Coventry university, UK, 2-3 September 2021: Academic Conferences International (ACI), 2021, pp. 484–491. doi: 10.34190/EKM.21.150.

[3] F. Bjørheim and I. M. La Torraca Lopez, “Tension testing of additively manufactured specimens of 17-4 PH processed by Bound Metal Deposition,” *1201*, 2021, Accessed: Jan. 26, 2024. [Online]. Available: https://uis.brage.unit.no/uis-xmlui/handle/11250/3011123

[4] Equinor, “3D printing and metal additive manufacturing (AM).” Accessed: Jan. 30, 2024. [Online]. Available: https://www.equinor.com/energy/3d-printing

[5] EOS, “Siemens counts on EOS Additive Manufacturing,” EOS GmbH. Accessed: Jun. 13, 2024. [Online]. Available: https://www.eos.info/en-us/industries/customer-success-stories/siemens-3d-printing-turbine-repair-burner

[6] T. Bellezze, A. Forcellese, P. Forcellese, T. Mancia, and M. Simoncini, “Effect of printing orientation on mechanical properties of components in stainless steel obtained using the Bound Metal Deposition technology,” *Procedia CIRP*, vol. 118, pp. 694–698, 2023, doi: 10.1016/j.procir.2023.06.119.

[7] H. Javidrad, B. Koc, H. Bayraktar, U. Simsek, and K. Gunaydin, “Fatigue performance of metal additive manufacturing: a comprehensive overview,” *Virtual Phys. Prototyp.*, vol. 19, no. 1, 2024, doi: 10.1080/17452759.2024.2302556.

[8] A. Fatemi *et al.*, “Fatigue behaviour of additive manufactured materials: An overview of some recent experimental studies on Ti-6Al-4V considering various processing and loading direction effects,” *Fatigue Fract. Eng. Mater. Struct.*, vol. 42, no. 5, pp. 991–1009, 2019, doi: 10.1111/ffe.13000.

[9] M. N. James *et al.*, “Residual stresses and fatigue performance,” *Eng. Fail. Anal.*, vol. 14, no. 2, pp. 384–395, 2007, doi: 10.1016/j.engfailanal.2006.02.011.

[10] X. Peng, L. Kong, J. Y. H. Fuh, and H. Wang, “A Review of Post-Processing Technologies in Additive Manufacturing,” *J. Manuf. Mater. Process.*, vol. 5, no. 2, Art. no. 2, 2021, doi: 10.3390/jmmp5020038.

[11] S. Sun, M. Brandt, and M. Easton, “2 - Powder bed fusion processes: An overview,” in *Laser Additive Manufacturing*, in Woodhead Publishing Series in Electronic and Optical Materials. , Woodhead Publishing, 2017, pp. 55–77. doi: 10.1016/B978-0-08-100433-3.00002-6.

[12] P. Yang *et al.*, “Effect of Printing Orientation on the Mechanical Properties of 3D-Printed Cu–10Sn Alloys by Laser Powder Bed Fusion Technology,” *Metals*, vol. 14, no. 6, Art. no. 6, 2024, doi: 10.3390/met14060660.

[13] A. Yadollahi, N. Shamsaei, S. M. Thompson, A. Elwany, and L. Bian, “Effects of building orientation and heat treatment on fatigue behavior of selective laser melted 17-4 PH stainless steel,” *Int. J. Fatigue*, vol. 94, pp. 218–235, 2017, doi: 10.1016/j.ijfatigue.2016.03.014.

[14] P. D. Nezhadfar, R. Shrestha, N. Phan, and N. Shamsaei, “Fatigue behavior of additively manufactured 17-4 PH stainless steel: Synergistic effects of surface roughness

and heat treatment," *Int. J. Fatigue*, vol. 124, pp. 188–204, 2019, doi: 10.1016/j.ijfatigue.2019.02.039.
[15] "Standard Specification for Precipitation-Hardening Stainless and Heat-Resisting Steel Plate, Sheet, and Strip." 2022.
[16] L. Carneiro, B. Jalalahmadi, A. Ashtekar, and Y. Jiang, "Cyclic deformation and fatigue behavior of additively manufactured 17–4 PH stainless steel," *Int. J. Fatigue*, vol. 123, pp. 22–30, 2019, doi: 10.1016/j.ijfatigue.2019.02.006.
[17] S. Sarkar, S. Mukherjee, C. S. Kumar, and A. Kumar Nath, "Effects of heat treatment on microstructure, mechanical and corrosion properties of 15-5 PH stainless steel parts built by selective laser melting process," *J. Manuf. Process.*, vol. 50, pp. 279–294, 2020, doi: 10.1016/j.jmapro.2019.12.048.
[18] H. Eisazadeh, S. Khadka, X. Wang, and P. Yuya, "A comparative study of the mechanical characteristics of additively and conventionally fabricated 17-4 precipitation hardened stainless steel," *Prog. Addit. Manuf.*, 2024, doi: 10.1007/s40964-024-00591-3.
[19] S. Kc, P. D. Nezhadfar, C. Phillips, M. S. Kennedy, N. Shamsaei, and R. L. Jackson, "Tribological behavior of 17–4 PH stainless steel fabricated by traditional manufacturing and laser-based additive manufacturing methods," *Wear*, vol. 440–441, 2019, doi: 10.1016/j.wear.2019.203100.
[20] J. O. Milewski, "Additive Manufacturing Metal, the Art of the Possible," in *Additive Manufacturing of Metals: From Fundamental Technology to Rocket Nozzles, Medical Implants, and Custom Jewelry*, vol. 258, in Springer Series in Materials Science, vol. 258. , Cham: Springer International Publishing, 2017, pp. 7–33. doi: 10.1007/978-3-319-58205-4_2.
[21] I. La Torraca, "Material characteristics of 3-D printed steel," Master thesis, University of Stavanger, 2021. Accessed: Feb. 07, 2024. [Online]. Available: https://uis.brage.unit.no/uis-xmlui/handle/11250/2784201
[22] J. Lu, L. Chang, J. Wang, L. Sang, S. Wu, and Y. Zhang, "In-situ investigation of the anisotropic mechanical properties of laser direct metal deposition Ti6Al4V alloy," *Mater. Sci. Eng. A*, vol. 712, pp. 199–205, 2018, doi: 10.1016/j.msea.2017.11.106.
[23] C. Qiu, N. J. E. Adkins, and M. M. Attallah, "Microstructure and tensile properties of selectively laser-melted and of HIPed laser-melted Ti–6Al–4V," *Mater. Sci. Eng. A*, vol. 578, pp. 230–239, 2013, doi: 10.1016/j.msea.2013.04.099.
[24] A. S. Johnson, S. Shao, N. Shamsaei, S. M. Thompson, and L. Bian, "Microstructure, Fatigue Behavior, and Failure Mechanisms of Direct Laser-Deposited Inconel 718," *JOM*, vol. 69, pp. 597–603, 2016, doi: 10.1007/s11837-016-2225-2.
[25] D. Tang, X. He, B. Wu, L. Dang, H. Xin, and Y. Li, "Anisotropic fatigue performance of directed energy deposited Ti-6Al-4V: Effects of build orientation," *Mater. Sci. Eng. A*, vol. 876, 2023, doi: 10.1016/j.msea.2023.145112.
[26] T. Muslim, T. Karagoz, S. Kurama, P. Sezer, O. F. Yazici, and R. Ozkok, "Laser metal deposition of 17–4 PH stainless steel: Geometrical, microstructural, and mechanical properties investigation for structural applications," *CIRP J. Manuf. Sci. Technol.*, vol. 41, pp. 69–79, 2023, doi: 10.1016/j.cirpj.2022.12.010.
[27] K. Riener, S. Oswald, M. Winkler, and G. J. Leichtfried, "Influence of storage conditions and reconditioning of AlSi10Mg powder on the quality of parts produced by laser powder bed fusion (LPBF)," *Addit. Manuf.*, vol. 39, 2021, doi: 10.1016/j.addma.2021.101896.
[28] T. C. Henry, M. A. Morales, D. P. Cole, C. M. Shumeyko, and J. C. Riddick, "Mechanical behavior of 17-4 PH stainless steel processed by atomic diffusion additive manufacturing," *Int. J. Adv. Manuf. Technol.*, vol. 114, no. 7, pp. 2103–2114, 2021, doi: 10.1007/s00170-021-06785-1.

[29] Markforged, “The Markforged Metal Additive Manufacturing Process.” Accessed: Feb. 06, 2024. [Online]. Available: https://markforged.com/resources/learn/design-for-additive-manufacturing-metals/metal-additive-manufacturing-introduction/metal-additive-manufacturing-process
[30] D. Metal, “Deep Dive: Bound Metal Deposition (BMD).” Accessed: Feb. 06, 2024. [Online]. Available: https://www.desktopmetal.com/resources/deep-dive-bmd
[31] Markforged, “Markforged Metal 3D Printer: The Metal X 3D Printing System.” Accessed: Feb. 05, 2024. [Online]. Available: https://markforged.com/3d-printers/metal-x
[32] Markforged, “Metal 3D Printing Design Tips.” Accessed: Feb. 26, 2024. [Online]. Available: https://markforged.com/resources/learn/design-for-additive-manufacturing-metals
[33] B. Iacopo, D. P. Valerio, M. Tommaso, P. Massimiliano, and V. Alessio, “Environmental impacts assessment of Bound Metal Deposition 3D printing process for stainless steel,” *Procedia CIRP*, vol. 105, pp. 386–391, 2022, doi: 10.1016/j.procir.2022.02.064.
[34] A. Watson, J. Belding, and B. D. Ellis, “Characterization of 17-4 PH Processed via Bound Metal Deposition (BMD),” presented at the TMS 2020 149th Annual Meeting & Exhibition Supplemental Proceedings, in The Minerals, Metals & Materials Series. February 23-27, 2020, San Diego, California, USA: Springer International Publishing, 2020, pp. 205–216. doi: 10.1007/978-3-030-36296-6_19.
[35] M. Gabilondo, X. Cearsolo, M. Arrue, and F. Castro, “Influence of Build Orientation, Chamber Temperature and Infill Pattern on Mechanical Properties of 316L Parts Manufactured by Bound Metal Deposition,” *Materials*, vol. 15, no. 3, Art. no. 3, 2022, doi: 10.3390/ma15031183.
[36] B. D. Lawrence, T. C. Henry, F. Phillips, J. Riddick, and A. Kudzal, “High-cycle tension-tension fatigue performance of additively manufactured 17–4 PH stainless steel,” *Int. J. Adv. Manuf. Technol.*, vol. 126, pp. 777–786, 2023, doi: 10.1007/s00170-023-11146-1.
[37] “Standard Test Methods for Tension Testing of Metallic Materials.” 2022.
[38] F. Bartolomeu *et al.*, “316L stainless steel mechanical and tribological behavior—A comparison between selective laser melting, hot pressing and conventional casting,” *Addit. Manuf.*, vol. 16, pp. 81–89, 2017, doi: 10.1016/j.addma.2017.05.007.
[39] T. T. Opoz, A. Burgess, J. I. Ahuir-Torres, H. R. Kotadia, and S. Tammas-Williams, “The effect of surface finish and post-processing on mechanical properties of 17-4 PH stainless steel produced by the atomic diffusion additive manufacturing process (ADAM),” *Int. J. Adv. Manuf. Technol.*, vol. 130, no. 7, pp. 4053–4066, 2024, doi: 10.1007/s00170-024-12949-6.
[40] M. A. Bouaziz, J. M. Djouda, M. Chemkhi, M. Rambaudon, J. Kauffmann, and F. Hild, “Heat treatment effect on 17-4PH stainless steel manufactured by Atomic Diffusion Additive Manufacturing (ADAM),” *Procedia CIRP*, vol. 104, pp. 935–938, 2021, doi: 10.1016/j.procir.2021.11.157.
[41] Per Kristian Larsen, “Utmatting,” in *Dimensjonering av stålkonstruksjoner*, 3., Bergen: Fagbokforlaget, 2020, pp. 479–524.
[42] M. Åman, Y. Tanaka, Y. Murakami, H. Remes, and G. Marquis, “Fatigue strength evaluation of small defect at stress concentration,” *Procedia Struct. Integr.*, vol. 7, pp. 351–358, 2017, doi: 10.1016/j.prostr.2017.11.099.
[43] Y. Peng and X. Zhu, “Fatigue strength estimation of butt-welded joints between cast-steel and hot-rolled-steel plates,” *Journal of Constructional Steel Research*, vol. 214, 2024, doi: 10.1016/j.jcsr.2024.108493.

[44] A. Ma, J. V. Sharp, and HSE, “Fatigue design of cast steel nodes in offshore structures based on research data.,” *Proc. Inst. Civ. Eng. - Water Marit. Energy*, vol. 124, no. 2, pp. 112–126, 1997, doi: 10.1680/iwtme.1997.29774.
[45] Sverdrup Steel, “EN 1.4542 / 17-4 PH.” Accessed: Jun. 14, 2024. [Online]. Available: https://www.sverdrupsteel.com/products/martensitic-alloys/alloy-1-4542-17-4-ph
[46] Markforged, “17-4 PHv2 stainless steel.” 2023. Accessed: Feb. 13, 2024. [Online]. Available: https://s3.amazonaws.com/mf.product.doc.images/Datasheets/Material+Datasheets/17-4PH-v2-SS-Datasheet.pdf
[47] J. R. Davis, *Tensile Testing, 2nd Edition*, 2nd ed. ASM International, 2004.
[48] Zwick Roell, “High cycle fatigue test & S-N test: DIN 50100,ASTM E466-15,ISO 1099.” Accessed: Feb. 16, 2024. [Online]. Available: https://www.zwickroell.com/industries/materials-testing/fatigue-test/high-cycle-fatigue-test-s-n-test-din-50100/
[49] INSTRON, “Dynamic Testing.” Accessed: Feb. 16, 2024. [Online]. Available: https://www.instron.com/en/resources/test-types/dynamic-test
[50] “Standard Practice for Conducting Force Controlled Constant Amplitude Axial Fatigue Tests of Metallic Materials.” 2021.